THE PI3-KINASE/TSC PATHWAY: A ROLE IN NEURAL AND RENAL DEVELOPMENT AND PATHOLOGY

APPROVED BY SUPERVISORY COMMITTEE

Luis F. Parada, Ph.D.

Jane E. Johnson, Ph.D.

Helmut Kramer, Ph.D

Robert E. Hammer, Ph.D.

TO

MY HUSBAND WENHUA GAO

AND MY PARENTS

ACKNOWLEDGMENTS

I am extremely thankful to Dr. Luis F. Parada, who is not only a great scientist but also a true mentor. He has great insights in his field, and at the same time he is open-minded and always encourages me to explore new fields. He has been very supportive on my projects and inspired me a lot throughout the past several years. More importantly, he values other people's opinions and encourages students to express their own thoughts even when there is a disagreement with his own. He also encourages students to attend conferences and meetings to broaden their knowledge and keep them updated with recent advances in the field. Thinking retrospectively, I feel I am lucky to have joined his lab and become his student.

I would like to thank my committee members, Drs. Jane E. Johnson, Helmut Kramer and Robert E. Hammer for their advice. They have been very positive about my research work during the past several years and gave me many useful suggestions.

I would also want to thank everyone in Dr. Parada's lab. They have always been very friendly and generous, which added considerably to my enjoyment in the lab. Particularly, I thank Dr. Chang-Hyuk Kwon for many helpful discussions and Gayatri Shrikhande and Yanjiao Li for their technical

support. I thank former lab members, Drs. Lei Lei, Bryan Luikart and Sharon A. Matheny, for their useful advice.

My gratitude also goes to my collaborators. I thank Drs. Craig Powell and Jacqueline Blundell for the behavioral tests, Drs. Shiori Ogawa and Christopher Sinton for EEG analysis, and Dr. James Brugarolas for many insightful suggestions on the kidney project.

Finally, I give my greatest thanks to my parents, my sister and my husband. It is their support and love that make my graduation today possible.

THE PI3-KINASE/TSC PATHWAY: A ROLE IN NEURAL AND RENAL DEVELOPMENT AND PATHOLOGY

By

JING ZHOU

DISSERTATION

Presented to the Faculty of the Graduate School of Biomedical Sciences

The University of Texas Southwestern Medical Center at Dallas

In Partial Fulfillment of the Requirements

For the Degree of

DOCTOR OF PHILOSOPHY

The University of Texas Southwestern Medical Center at Dallas

Dallas, Texas

July, 2008

THE PI3-KINASE/TSC PATHWAY: A ROLE IN NEURAL AND RENAL DEVELOPMENT AND PATHOLOGY

Jing Zhou, Ph.D.

The University of Texas Southwestern Medical Center at Dallas, 2008

Luis F. Parada, Ph.D.

PTEN is a tumor suppressor gene and its protein product negatively regulates the PI3K/AKT pathway through counteracting the kinase function of PI3-Kinase. Loss of function of PTEN results in overactivation of AKT and in turn activates multiple AKT downstream pathways. One AKT substrate is the TSC1/2 protein complex, which controls protein synthesis and cell growth through regulating mTOR activity. AKT inhibits TSC1/2 complex by directly phosphorylating TSC2, and in turn releases the inhibition of TSC1/2 complex on mTOR. Thus, loss of either PTEN or TSC1 or TSC2 can result in increased mTOR activity. However, regulation of TSC1/2 complex by AKT could be context dependent and the TSC/mTOR pathway is regulated by upstream regulators other than AKT in different cell types. In this study, I characterized the

functions of PTEN and TSC1 in both post-mitotic neurons and renal tubule cells, and evaluated the relationship of these two tumor suppressor genes in two distinct contexts.

Previously, a conditional *Pten* knockout mouse line was generated with *Pten* loss in limited post-mitotic neurons in the cortex and hippocampus. These mice develop macrocephaly accompanied by neuronal hypertrophy and loss of neuronal polarity. The mutant mice also exhibit behavioral abnormalities reminiscent of certain features of human autism. Biochemical analysis indicates that multiple AKT downstream pathways including the TSC/mTOR pathway are activated in neurons that lose *Pten*. In the current study, I demonstrate that rapamycin, a specific inhibitor of mTOR, can prevent or reverse neuronal hypertrophy resulting in the amelioration of PTEN-associated abnormal behaviors. In addition, loss of *Tsc1* in a same context results in similar neuronal hypertrophy. Thus, the study provides evidence that the mTOR pathway is critical for the neuronal phenotype observed in *Pten* mutant mice.

In the second part of the study, I demonstrate that severe polycystic kidneys disease develops in *Tsc1* mutant mice, but not in *Pten* mutant mice. Apparently, overactivation of mTOR signaling only occurs in the kidneys of *Tsc1* mutant mice, suggesting distinct activities for PTEN and TSC1 in mTOR activation in renal tubule cells compared to that found in neurons.

TABLE OF CONTENT

LIST OF PUBLICATIONS

1. **Zhou, J.**, Brugarolas, J., and Parada, L.F. *Tsc1* mediated polycystic kidney disease. (in preparation) 2008.

2. **Zhou, J.**, Blundell, J., Ogawa, S., Kwon, C.H., Zhang, W., Sinton, C., Powell, C.M. and Parada, L. F. Pharmacological inhibition of mTOR suppresses anatomical, cellular and behavioral deficiencies in neural specific *Pten* knock out mice. (in submission) 2008.

3. Ogawa, S., Kwon, C. H., **Zhou, J**., Koovakkattu, D., Parada, L. F., and Sinton, C. M. (2007). A seizure-prone phenotype is associated with altered free-running rhythm in Pten mutant mice. Brain Res *1168*, 112-123.

4. Kwon, C. H., Luikart, B. W., Powell, C. M., **Zhou, J.**, Matheny, S. A., Zhang, W., Li, Y., Baker, S. J., and Parada, L. F. (2006). Pten Regulates Neuronal Arborization and Social Interaction in Mice. Neuron *50*, 377-388.

5. Kwon, C. H., **Zhou, J.**, Li, Y., Kim, K. W., Hensley, L. L., Baker, S. J., and Parada, L. F. (2006). Neuron-specific enolase-cre mouse line with cre activity in specific neuronal populations. Genesis *44*, 130-135.

6. Lei, L., **Zhou, J.**, Lin, L., and Parada, L. F. (2006). Brn3a and Klf7 cooperate to control TrkA expression in sensory neurons. Dev Biol *300*, 758-769.

7. Lei, L., Laub, F., Lush, M., Romero, M., **Zhou, J.**, Luikart, B., Klesse, L., Ramirez, F., and Parada, L. F. (2005). The zinc finger transcription factor Klf7 is required for TrkA gene expression and development of nociceptive sensory neurons. Genes Dev *19*, 1354-1364.

8. Guo, C., Fischhaber, P. L., Luk-Paszyc, M. J., Masuda, Y., **Zhou, J**., Kamiya, K., Kisker, C., and Friedberg, E. C. (2003). Mouse Rev1 protein interacts with multiple DNA polymerases involved in translesion DNA synthesis. Embo J *22*, 6621-6630.

9. **Zhou, J**., Cheng, S. C., Luo, D., and Xie, Y. (2001). Study of multi-drug resistant mechanisms in a taxol-resistant hepatocellular carcinoma QGY-TR 50 cell line. Biochem Biophys Res Commun *280*, 1237-1242.

LIST OF FIGURES

LIST OF TALBES

LIST OF ABBREVIATIONS

ASDs	autism spectrum disorders
BUN	blood urea nitrogen
BrdU	5-bromo-2-deoxyuridine
CNS	central nervous system
EDTA	ethylenediaminetetraacetic acid
EEG/EMG	electroencephalogram/electromyogram
FACS	fluorescence-activated cell sorting
FKBP12	FK506-binding protein
FXS	fragile X syndrome
GAP	GTPase-activating protein
GTP	guanosine-5'-triphosphate
IHC	immunohistochemistry
i.p.	intraperitoneally
IRS	insulin receptor substrate
LTA	lotus tetragonolobus agglutinin
MeCP2	methyl-CpG binding protein 2
ML	molecular layer
mTOR	mammalian target of rapamycin
PAGE	polyacrylamide gel electrophoresis
PBS	phosphate-buffer saline
PDD	pervasive developmental disorders
PDK1	phosphoinositide-dependent kinase 1
PKD	Polycystic kidney disease
PIKK	phosphatidylinositol kinase-related kinase
PIP2	phosphotidylinosital-4,5-triphosphate
PIP3	phosphotidylinosital-3,4,5-triphosphate

PI3K	phosphatidylinositol 3-kinase
PTEN	phosphatase and tensin homolog deleted on chromosome ten
RTKs	receptor tyrosine kinases
RTT	Rett syndrome
SH2 domain	Src homology 2 domain
S6K1	ribosome protein S6 kinase
TOP	track of oligopyrimidine
TOR	target of rapamycin
TORC1	TOR complex 1
TORC2	TOR complex 2
TSC	tuberous sclerosis complex
X-gal	5-bromo-4-chloro-3-indolyl-b-D-galactopyranoside
YFP	yellow Fluorescent Protein
4E-BP1	eukaryotic initiation 4E-binding protein 1

Chapter I: General Introduction

PI3K/PTEN/AKT and TSC/mTOR pathway

PI3K/PTEN/AKT pathway

The PI3K/PTEN/AKT pathway is a well recognized biochemical pathway that responds to extracellular signals via either receptor tyrosine kinases (RTKs) or G-protein coupled receptors. How this pathway is activated *in vivo* might depend on the identity of upstream receptors and vary in details, but in general it follows several key steps.

Taking RTKs as an example (refer to Figure 1.1), upon ligand binding, RTKs are autophosphorylated at their cytoplasmic tails, which in turn activate the downstream cascades including phosphatidylinositol 3-kinase (PI3K). PI3K is a heterodimer that consists of a regulatory p85 subunit and a catalytic p110 subunit. Through interaction with the p85 subunit, phosphorylated cytoplasmic tails of RTKs are capable of recruiting p85/p110 complex to the cellular membrane, resulting in the activation of p110. The p85-RTK interaction can be either direct or indirect; in some cases, the SH2 domain of p85 subunit binds to the phosphotyrosine residues of active RTKs; in other cases, like insulin receptors, p85-RTK binding is indirect and occurs through intermediate phosphoproteins called insulin receptor substrates (IRSs).

The primary consequence of PI3K activation is production of phosphotidylinosital-3,4,5-triphosphate (PIP3) from phosphotidylinosital-4,5-triphosphate (PIP2) on the plasma membrane. Generation of PIP3 in turn recruits the serine/threonine kinase phosphoinositide-dependent kinase 1

(PDK1) and AKT (also known as protein kinase B, PKB) to the plasma membrane, where AKT is activated through PDK1 phosphorylation at Thr308 (Alessi et al., 1997; Stokoe et al., 1997). The full activation of AKT also depends on phosphorylation of Ser473 (Alessi et al., 1996), which will be discussed later.

AKT was initially discovered as an oncogene from the mouse AKT8 retrovirus (Staal, 1987) and later was recognized as an important serine/threonine kinase that belongs to the AGC kinase family (Bellacosa et al., 1991; Jones et al., 1991). In the last two decades, its cellular functions have been extensively studied. To date, a handful of AKT substrates have been identified, including GSK3, BAD, FOXO, Caspase 9, MDM2 and p21 (refer to Table 1.1 for a more complete list) (Manning and Cantley, 2007). These AKT substrates are broadly involved in various intracellular signal transduction pathways, which empower AKT to regulate multiple cellular functions, including cell survival, cell growth, cell metabolism and cell migration (Manning and Cantley, 2007; Vivanco and Sawyers, 2002).

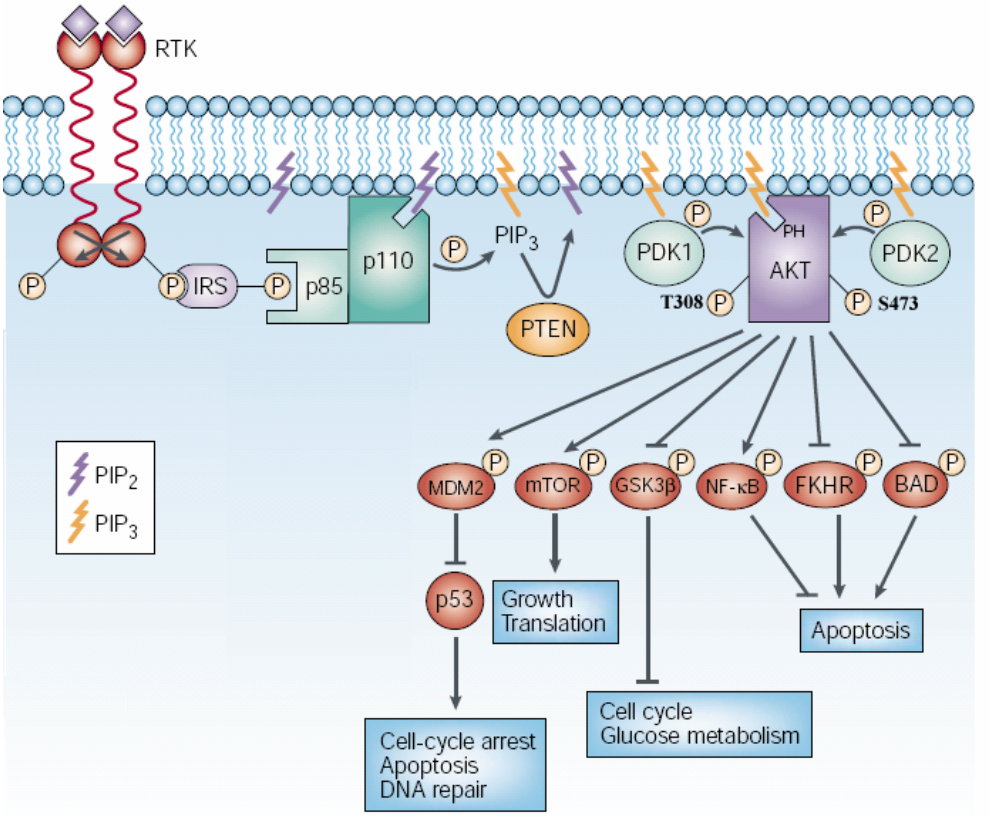

Figure 1.1 Activation of the PI3K/PTEN/AKT pathway. (Adapted and modified from review of Vivanco & Sawyers, Nature, 2002).

Table 1.1 List of identified AKT substrates. (Adapted from review of Manning and Cantley, Cell, 2007)

Table 1. Characteristics and Experimental Evidence for a Subset of Akt Substrates[a]

Target	Human Site(s)[b]	In Vitro[c]	In Vivo[d]			Genetic Evidence[e]	Regulatory Effect?[f]
			W/L	LOF	GOF		
FOXO1	T24, S256, S319	+	+	+	+	M, F, W	Inhibit
FOXO3A	T32, S253, S315	+	+	+	+	M, F, W	Inhibit
FOXO4	T32, S197, S262	+	+	+	+	M, F, W	Inhibit
TSC2	S939, T1462	+	+	+	+	M, F	Inhibit
GSK3α/β	S21/S9	+	+	+	+	M	Inhibit
RAF1	S259	+	+	+	+	–	Inhibit
PRAS40	T246	+	+	–	+	M	Inhibit
AS160	S588, T642	+	+	–	–	–	Inhibit
BAD	S99	+	+	+	+	–	Inhibit
WNK1	T60	+	+	+	–	M	?
MDM2	S166, S186	+	+	+	+	–	Activate
Chk1	S280	+	+	+	+	M	Inhibit
eNOS	S1177	+	+	+	+	M	Activate
ASK1	S83	+	+	+	+	–	Inhibit
IKKα	T23	+	–	–	–	–	Activate
p21CIP1	T145	+	+	+	+	–	Inhibit
p27KIP1	T157	+	+	+	+	–	Inhibit
Casp9	S196	+	–	+	+	–	Inhibit

[a]For an expanded version of this table see Table S1.
[b]Human numbering of sites with strongest evidence of being phosphorylated by Akt in vivo.
[c]Direct phosphorylation of the given site(s) with purified Akt and full-length substrate in vitro.
[d]Evidence of Akt-dependent phosphorylation of the given site(s) within cells (– means no published evidence), including: W/L, sensitivity to PI3K inhibition using ≤ 100 nM wortmannin (W) and/or ≤ 20 μM LY294002 (L); LOF, loss-of-AKT-function evidence using dominant-negative mutants and/or RNAi approaches; GOF, gain-of-Akt-function evidence using overexpression and/or constitutively active mutants.
[e]Genetic evidence in model organisms, including epistasis analyses in *Drosophila* (F) or *C. elegans* (W) or loss-of-phosphorylation in mouse mutants (M) lacking Akt function.
[f]Functional consequence of Akt-mediated phosphorylation.

PTEN (phosphatase and tensin homolog deleted on chromosome ten) is probably the most important negative regulator of PI3K/AKT signaling that has been discovered so far. PTEN was first identified as a tumor suppressor gene mainly in glioma and breast cancer cell lines (Li et al., 1997; Steck et al., 1997). After that, PTEN's function as a phosphatase was soon recognized and established. Although PTEN might be able to dephosphorylate proteins, the well acknowledged role of PTEN is as a lipid phosphatase (Maehama and Dixon, 1998). PTEN is able to dephosphorylate PIP3 to PIP2 at the D3 position, directly counter-acting the function of PI3K (refer to Figure 1.2) (Sansal and Sellers, 2004). Therefore, in the absence of PTEN, PIP3 accumulates and AKT is over activated, a situation that occurs in many human cancers (Ali et al., 1999).

The function of the PI3K/PTEN/AKT pathway can be context-dependent. For example, in the nervous system, it has been shown that deletion of *Pten* in stem cells or astrocyte populations resulted in both cellular hypertrophy and increased proliferation (Fraser et al., 2004; Groszer et al., 2001). Whereas, if the loss of *Pten* is restricted to postmitotic neurons, the main consequence is hypertrophy in the absence of proliferation (Backman et al., 2001; Kwon et al., 2001). Thus, context-dependent PTEN function may reflect the activation of distinct downstream pathways in different circumstances or the cross-talk with other signaling pathways.

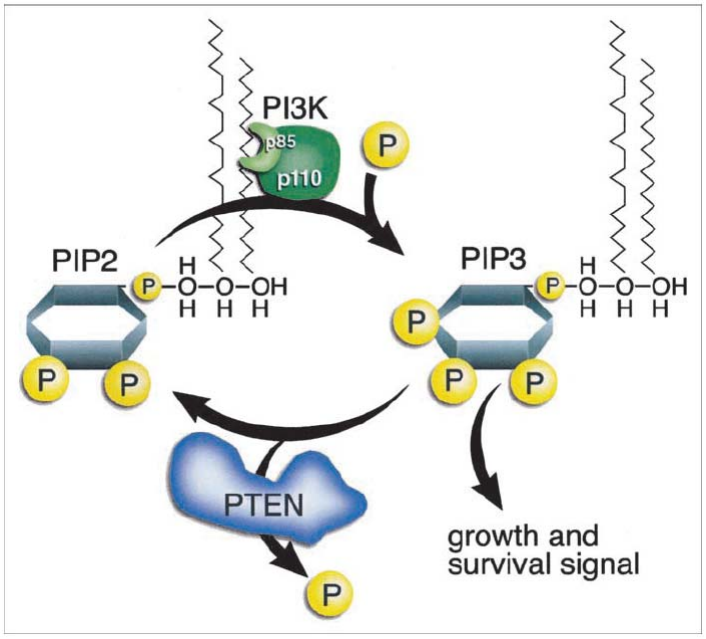

Figure 1.2 PTEN is a lipid phosphatase that counteracts the kinase function of PI3K. (Adapted from review of Sansal and Seller, Journal of Clinical Oncology, 2004)

Rapamycin and mTOR signaling

The discovery of TSC/mTOR signaling is related to the discovery of rapamycin, a drug that was initially isolated from the soil of Easter Island for its antifungal activity in the 1970s (Vezina et al., 1975). The structure of rapamycin is shown in Figure 1.3. The cellular target of rapamycin (TOR) was later identified from the yeast bearing mutations that were resistant to rapamycin (Heitman et al., 1991). As we now know, there are two TOR genes identified in yeast, while mammals only possess a single TOR gene, named mTOR (mammalian target of rapamycin).

Rapamycin is able to inhibit the proliferation and growth of mammalian cells and is clinically used as an immunosuppressant. Today, we have a clearer picture of how it works. Studies suggest that its activity requires an endogenous co-factor, FKBP12 (Sabatini et al., 1994). In fact, rapamycin binds to FKBP12 protein to form a complex first and then interacts and perturbs the function of TOR. However, the intrinsic function of FKBP12 protein is not clear.

TOR is a large molecule (~280kDa) that belongs to the phosphatidylinositol kinase-related kinase (PIKK) family. Although it contains a lipid kinase-like domain, TOR, like other members in this family, does not possess lipid kinase activity, but instead functions as a serine/threonine kinase. However, TOR has to associate with different cofactors in order to function. There are two TOR complexes in both yeast and mammals, TOR complex 1 (TORC1) and TOR complex 2 (TORC2) (Wullschleger et al., 2006). In

mammals, mTORC1 contains mTOR, raptor and mLST8 (also known as GβL). While mTORC2 contains mTOR and mLST8, but instead of raptor, it associates with a different protein called rictor. Interestingly, only TORC1 is rapamycin sensitive, that is, rapamycin-FKBP12 complex interferes with the function of TORC1 only, but not TORC2.

Between these two TOR complexes, TORC1 is the better understood. In mammalian cells, mTORC1 exerts its effects on controlling protein synthesis by two major downstream effectors: ribosome protein S6 kinase-1(S6K1) and eukaryotic initiation 4E-binding protein 1(4E-BP1). In many cases, loss of S6K1 was found to result in reduced cell size, which mimics the effect of rapamycin. S6K1 could be activated by mTOR through direct phosphorylation, which then activates the 40S ribosomal protein S6. Previously, this was thought to lead to increased translation of a subset of mRNA with 5' track of oligopyrimidine (TOP). However, this model is challenged by recent studies that indicate neither S6K1 nor S6 phosphorylation is required for the translation of 5' TOP mRNA (Pende et al., 2004; Stolovich et al., 2002). Therefore, S6K1 might control cell size via other machineries, which is not clear right now. On the other hand, mTOR could phosphorylate 4E-BP1 and release its inhibition on eIF4E, therefore, promoting the cap-dependent translation (Richter and Sonenberg, 2005). Besides translation, mTOR also plays roles in regulating ribosome biogenesis, autophagy and transcription (Wullschleger et al., 2006), which will not be discussed here.

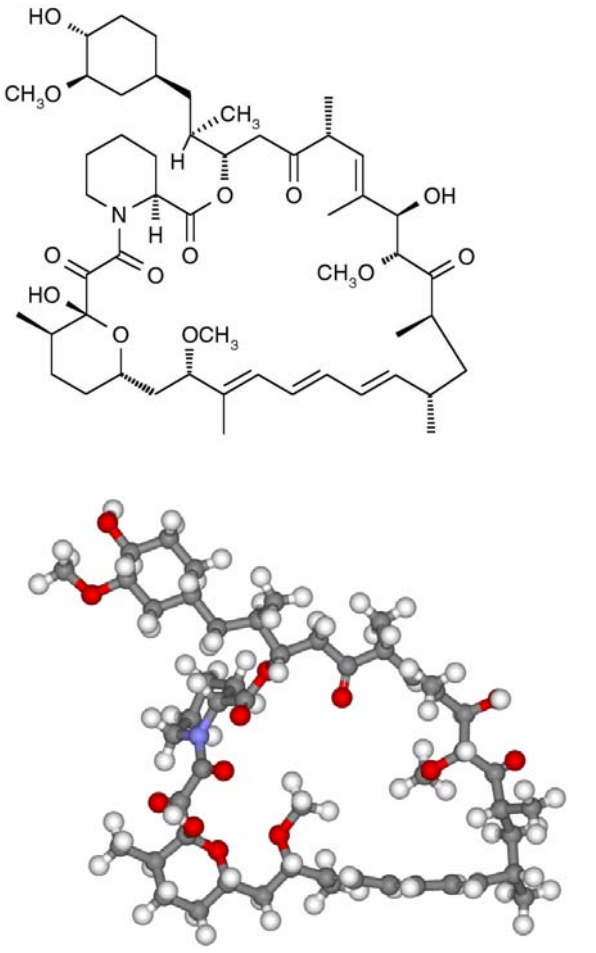

Figure 1.3 Structure of rapamycin (also known as sirolimus) reveals that rapamycin is a macrolide compound. (Images is adapted from http://en.wikipedia.org/wiki/Rapamycin)

TSC/TOR is regulated by AKT

Interestingly, it had been known for some time that TOR activity is regulated by AKT activation, although how this process occurs was not known. Until recent years, studies suggested that AKT is capable of activating TORC1 through tuberous sclerosis complex (TSC) (Figure 1.4).

Clinically, TSC refers to a genetic disorder that is characterized by hamartomas derived from multiple organs, including brain, kidney, skin and liver. It is a rare disease with prevalence of 1:10,000 live births (Osborne et al., 1991). It is genetically linked to mutations of either the TSC1 or TSC2 gene that encode protein hamartin or tuberin respectively (1993; van Slegtenhorst et al., 1997). These two proteins function together as a TSC1/2 complex. Recently, this complex is shown to possess GTPase-activating protein (GAP) activity for the ras-family GTP-binding protein Rheb (Garami et al., 2003; Saucedo et al., 2003; Stocker et al., 2003; Tee et al., 2003; Zhang et al., 2003), which is capable of directly binding to and activating TORC1 (Long et al., 2005). Therefore, through downregulation of Rheb, the TSC1/2 complex negatively regulates TORC1 and its downstream effectors.

AKT regulates TORC1 through TSC1/2 complex. It has been reported by three independent groups that AKT directly phosphorylates TSC2 to inhibit the activity of TSC1/2 complex (Inoki et al., 2002; Manning et al., 2002; Potter et al., 2002). Therefore, with AKT activation, it releases the inhibitory effect of TSC1/2 complex on TORC1, which explains in many cases the effect

of AKT on promoting cell growth. Thus, TSC/mTOR pathway has been recognized as one of the important downstream mediators of AKT function.

However, we have to point out here that the relationship between PI3K/PTEN/AKT and TSC/mTOR pathway is not always linear and could be complicated depending on the context. Their relationship should always be considered at several levels.

First, TSC/mTOR is one of the downstream pathways of AKT. As discussed above, mTOR signaling was initially identified for its response to growth stimulation and AKT activity. Clinically, some of PTEN associated tumors, such as Cowden's disease, Lhermitte-Duclos disease, and Bannayan-Zonana syndrome, all demonstrate hamartoma syndrome that is similar to TSC patients, suggesting the involvement of dysregulation of mTOR signaling. But on the other hand, mutations of *PTEN* were linked to a broader spectrum of cancers in human, including brain cancer, breast cancer and prostate cancer, which might reflect the activation of other downstream pathways of AKT.

Second, TSC/mTOR conducts signals independent of the PI3K/PTEN/AKT pathway. As AKT exerts its effects through multiple substrates, today we realize that TSC/mTOR not only responds to growth factors, but also integrates various extra- and intra-cellular signals *in vivo*, including growth factors, nutrients, energy status and stress, via different upstream regulatory pathways (Tee and Blenis, 2005; Wullschleger et al., 2006). Clinically, harmatomas in TSC patients rarely progress to malignancy. However, renal cancers associated with TSC are exceptions, and are not

usually linked to *PTEN* mutations. The similarities and distinctions of *PTEN* and *TSC* associated manifestations suggest these two pathways might work in synergy or parallel depending on the context.

Third, there are feedback effects from mTOR signaling to the PI3K/PTEN/AKT pathway. One feedback loop is mediated by S6K1. It has been demonstrated that S6K1 represses upstream signaling of PI3K/AKT by directly phosphorylating IRS1 and inducing its subsequent degradation (Harrington et al., 2004; Shah et al., 2004; Um et al., 2004). More interestingly, studies suggest that TORC2 can efficiently phosphorylate AKT at Ser473 (Sarbassov et al., 2006; Sarbassov et al., 2005). This explains the observation that in some cases chronic rapamycin administration reduced AKT activity. Although mTORC2 is rapamycin-insensitive, long-term rapamycin treatment is believed to be able to sequester mTOR in mTORC1 and cause the depletion of mTOR from mTORC2, thereby negatively affecting AKT activity. However, this feedback effect is context-dependent, as *in vitro* not every cell line exposed to rapamycin results in downregulation of P-AKT-S473 level (Sarbassov et al., 2006).

Today, TSC/mTOR pathway is no longer considered simply as a downstream effector of AKT, but instead is considered more as an independent pathway that cross-talks with many other pathways including the PI3K/PTEN/AKT pathway. Thus, the relationship between PI3K/PTEN/AKT and TSC/mTOR has to be assessed depending on the specific context.

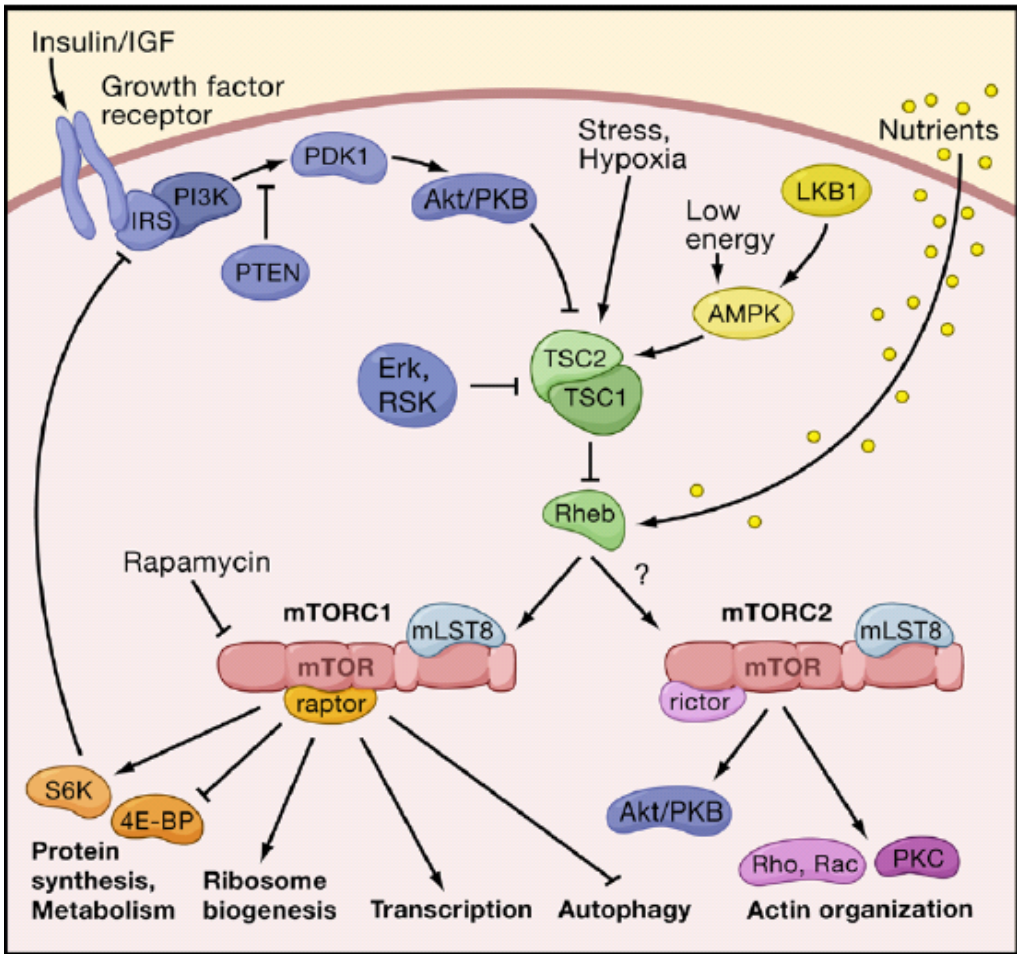

Figure 1.4 Relationship between the PI3K/PTEN/AKT and the TSC/mTOR pathways. (Adapted from review of Wullschleger *et al.*, Cell, 2006).

Autism and brain growth:

Autism spectrum disorders (ASDs)

Human autism spectrum disorders (ASDs) are complex neurodevelopmental disorders defined behaviorally by severe impairment of social interaction and communication, as well as restricted and repetitive movement and interest. It is also referred to as pervasive developmental disorders (PDD) according to the *Diagnostic and Statistical Manual of Mental Disorders (DSM-IV)* and clinically covers five conditions: 1) classic autism, 2) Asperger syndrome, 3) Rett syndrome, 4) childhood disintegrative disorders, and 5) pervasive developmental disorders—not otherwise specified (PDD-NOS). It has recently been estimated that as many as 3-6 per 1000 children are affected by ASDs with about 3:1 ratio between male and female (Bertrand et al., 2001; Fombonne, 2003; Yeargin-Allsopp et al., 2003). However, the etiology of autism is far from clear, which leads to no effective treatment.

ASDs are genetic brain disorders.

From studies of the past decades, we learned that ASDs are highly inheritable brain disorders. Although environmental factors cannot be excluded in the pathogenesis of ASDs, evidence suggests that ASDs have a strong genetic component. First, the recurrence rate of autism among affected siblings is 2-8%, which is much higher than the prevalence in the general population (Muhle et al., 2004). Secondly, the concordance for autism in

identical twins is 60-90% in contrast to only 0-10% among dizygotic twins (Bailey et al., 1995). Thus, these data suggest that ASDs are genetic disorders.

Searching the etiology of ASDs

To disclose the etiology of ASDs, a multidisciplinary approach has been used. Genetically, three approaches have been adopted for locating ASDs susceptibility genes: genome wide screens for linkage analysis in affected families, cytogenetic studies for chromosome abnormalities in autistic individuals, and selective candidate gene analysis. So far, several chromosome regions have been linked to autism, such as chromosome 2q, 7q and 15q, and up to 100 genes have been proposed to relate to autism (Klauck, 2006; Wassink et al., 2004). However, more associative studies have to be done to confirm causal relationships between these putative genes and ASDs.

Besides the genomic approaches mentioned above, neuropathology on postmortem tissues and functional MRI have also been proved useful for identifying brain regions, neuronal abnormalities and molecular bases putatively involved in ASDs. In addition, the autism associated manifestations sometimes offer clues or evidence that help to uncover the underlying mechanisms. For example, in the past, the study on rare diseases that overlap with autism, such as Rett syndrome (RTT), fragile X syndrome (FXS) and tuberous sclerosis, have offered a special angle to uncover the possible underlying mechanisms that contribute to pathogenesis of ASDs. Finally, the development and use of murine models have enabled the detailed study of

candidate genes for their associations with autism and their cellular functions, further offering opportunities for testing possible treatments.

Unfortunately, to date the etiology of ASD is still far from clear, resulting in an absence of effective strategies for medical treatment. We realize that ASDs are disorders with complex nature. The progress of pursuing pathogenesis of autism is partially hindered by the marked phenotypic diversity present in autism patients. As defined behaviorally, manifestations of ASDs have three core symptom domains: abnormal social interaction, deficits in verbal and nonverbal communication, and repetitive behaviors. Clinically, autism is frequently associated with additional symptoms as well. These include not only mental disorders, such as seizure, anxiety and sleep disorders, but also non-neuronal symptoms, like gastrointestinal and immunological symptoms (Aman and Langworthy, 2000; Canitano, 2007; Jyonouchi et al., 2005; Malow, 2004; Tuchman and Rapin, 2002; Valicenti-McDermott et al., 2006). As mentioned above, many other rare diseases overlap with autism, like Rett syndrome, fragile X syndrome and tuberous sclerosis. This phenotypic diversity correlates with the fact that identified susceptibility genes of ASDs have very diverse cellular functions, which are involved almost in every aspects of neuronal functions, from neuronal growth and migration to synaptic formation. It is also likely that pathogenesis of ASDs could be complicated by the involvement of multiple genetic factors.

Autism susceptibility genes

Here, we will try to briefly summarize the genes that have been associated with autism based on their different cellular functions, with an emphasis on components of PI3K/PTEN/AKT pathways. In addition, we will discuss a little bit of the data about the genes that are responsible for Rett syndrome and fragile X syndrome.

Autism and PI3K/AKT/mTOR pathway

It has been noticed for decades that autism is associated with abnormal brain growth. Interestingly, as reflected by brain circumference, both increased and decreased brain sizes have been reported among the autism population (Fombonne et al., 1999). Particularly, we noticed that several independent studies have suggested about 10-20% of autism patients have macrocephaly (Davidovitch et al., 1996; Deutsch and Joseph, 2003; Fidler et al., 2000; Lainhart, 2003; Lainhart et al., 1997; Piven et al., 1995; Stevenson et al., 1997). A recent review from Courchesne and his colleagues further suggests that overgrowth during early brain development could be one of the key factors in the pathogenesis of autism (Courchesne et al., 2007). Thus, one hypothesis would be that pathways controlling growth play a role in the etiology of autism. One good example will be the PI3K/AKT/mTOR pathway, which regulates cell growth and division.

Indeed, mutations of negative regulators of this pathway have been related to autism. Firstly, mutations in PTEN have been found to cause macrocephaly in both human and mouse. Further, increasing clinical reports

link germline PTEN mutations to a subset of autism patients with macrocephaly (Butler et al., 2005; Goffin et al., 2001; Herman et al., 2007) (summarized in Table 1.2). Today, screening for *PTEN* mutations in autism patients with macrocephaly is warranted. Consistent with these clinical reports, we have demonstrated previously that mice with *Pten* loss in post-mitotic neurons in the cortex and hippocampus develop macrocephaly and additional behavioral phenotypes reminiscent of human autism (Kwon et al., 2006a). Secondly, it has been known for decades that TSC patients also suffer from mental problems, including mental retardation, epilepsy and autism. Further, psychiatric and behavioral evaluations of TSC patients have reported a significant incidence of autism ranging from 25 to 50 percent of cases (Smalley, 1998; Smalley et al., 1992; Wiznitzer, 2004). All this information indicates that malfunction of the PI3K/AKT/mTOR pathway might be responsible for the pathogenesis of a subset of autism patients.

Table 1.2 Summary of clinical reports on autism patients with *PTEN* mutations.

Patient	Sex	Age (years) diagnosed as ASD	PTEN Mutations	Other	Reference
1	M	11	Axon 5, nonsense mutation R130X		Zori et al., Am J Med Genet. 1998
2	M	8	Axon 5, nonsense mutation R130X	Macrocephaly, mental retardation	Parisi et al., J Med Genet. 2001
3	M	8	Exon 6, nonsence mutation Y178X 534T>G	Macrocephaly, developmental delay	Goffin et al., Am J Med Genet. 2001
4	M	4	Exon 4, missense mutation CAT>CGT, H93R	Macrocephaly, speech delay	Bulter et al., J. Med. Genet. 2005
5	M	3.5	Axon 7, missense mutation GAC>GGC, D252G	Macrocephaly, developmental delay, speech apraxia	Bulter et al., J. Med. Genet. 2005
6	M	2.5	Axon 7, missense mutation TTT>TCT, F241S	Macrocephaly, development delay, seizure	Bulter et al., J. Med. Genet. 2005
7	F	~2.5	Axon 6, single base insertion 530insT, premature termination	Macrocephaly, developmental delay	Herman et al., Am J Med Genet A. 2007
8	M	4	Axon 5, nonsense mutation R130X	Macrocephaly, developmental delay	Herman et al., Am J Med Genet A. 2007
9	M	5	Axon 8, missense mutation D326N	Macrocephaly, mental retardation	Buxbaum et al., Am J Med Genet B. 2007

Autism and brain patterning genes:

Consistent with being neurodevelopmental disorders, ASDs have been associated with the abnormal brain organization, suggesting the involvement of the disruption of normal migration process. For example, REELIN, the gene located on chromosome 7q, one of the autism susceptibility chromosome regions, has been suggested to link to autism. As we knew, its function is involved in controlling neuronal migration in cerebral cortex, hippocampus, and cerebellum (Serajee et al., 2006). Similarly, the cerebellar development patterning gene ENGRAILED 2 has also been found to be associated with autism (Kuemerle et al., 2007).

Autism and synaptic genes:

A number of genes that function at synapses appear on the list of susceptibility genes of autism as well. The γ-amino butyric acid (GABAa) receptor subunit genes cluster is located on the 15q11-13 chromosome region that was associated with autism (Bolton et al., 2001). In addition, serotonin transporter gene (5-HTT) has been suspected to be associated with autism (Cook et al., 1997; Yirmiya et al., 2001). Finally, genes encoding neuroligin-3 and 4, members of post-synaptic cell-adhesion molecules, have been found mutated in a small percentage of autistic individuals (Jamain et al., 2003). Intriguingly, mice bearing

the same point mutation of nuroligin-3 as found in autism patients, show increased inhibitory synapses and impaired social behaviors (Tabuchi et al., 2007).

From rare diseases to autism:

In the past, study of rare diseases that overlap with autism have provided invaluable insight into understanding the biological mechanisms of idiopathic autism. Here, we just want to use two extensively studied autism related disorders as examples: Fragile X syndrome (FXS) and Rett syndrome (RTT).

FXS is caused by fragile X mental retardation 1 (FMR1) gene mutation, which clinically associated with a broad spectrum of mental manifestations including not only mental retardation, but also learning deficits and autism. Particularly, studies suggest that about 30-35% FXS patients show autistic phenotype, which counts for 2-6% among autism children (Hagerman, 2006; Hagerman et al., 2005). Therefore, screening for FMR1 gene mutation is warranted when examining autism patients. The cellular function of FMR1 protein has been extensively studied. Although there is still debate, it is known that FMR1 protein is an RNA binding protein that negatively regulates mRNA translation at the synapse, suggesting a role in controlling local protein synthesis and further synaptic activity. Examination of human FXS reveals increased long, thin and immature dendritic spines, indicating altered synaptic structure and function in FXS patients (Bagni and Greenough, 2005).

RTT is an X-linked dominant neurodevelopmental disorder. Today, Rett syndrome is classified under the autism spectrum disorders, together with a few other neurondevelopmental disorders including the classic autism and Asperger Syndrome. Compared to classic autism, RTT is rare and affects mainly girls with the prevalence of 1 in 10,000 to 15,000 in females (Percy, 2002). The clinical features of RTT suggest that it is a postnatal progressive neurodevelopment disorder. Patients diagnosed with RTT appear to develop normally until 6-18 months of age, and then start to develop deceleration of head growth accompanied with loss of acquired language, cognitive, social, and motor skills. Studies have shown that over 80% of cases of RTT are caused by mutations in the methyl-CpG binding protein 2 (MeCP2) gene (Amir et al., 1999), which is involved in regulating gene transcription. Some most recent advances on the MeCP2 functions have been extensively reviewed by Chahrour and Zoghbi (Chahrour and Zoghbi, 2007). Still, it is worth pointing out here that as a transcriptional regulatory protein, the target genes of MeCP2 are still under identified. On the other hand, it is still a mystery that both loss and gain of function of MeCP2 could result in the similar clinical manifestations.

A mechanism of balance

An intriguing question is: “By reviewing the identified genes that have been associated with autism, can we get a clue on the mechanisms that are

responsible for this social disorders?". This leads to the search for common cellular functions that are shared by the susceptibility genes. However, studies suggested controversial cellular effects of autism associated genes. We know mutations of PTEN causes macrocephaly, but RTT is more frequently associated with microcephaly. In contrast to reduced spine density observed in MeCP2 null neurons, increased spine density was reported in FMR1 and PTEN mutated neurons. Mutation of neuroligin 3 increases inhibitory synapse, whereas loss of GABAa receptor decreases it. All these observations offer clues, but also confuse us. Perhaps, the fact that the involvement of both loss and gain of function of MeCP2 in RTT already gives us a hint, that is, this is not about more or less, but a balance.

PKD and mTOR signaling

Kidney organization and renal development:

The kidney performs the essential function of removing waste from the blood. The gross structure of the kidney is shown in Figure 1.5. Anatomically, it contains three parts from the outside to inside: the cortex, medulla and renal pelvis. The basic functional unit of the kidney is nephron. As shown in Figure 1.5, each nephron consists of two parts: the renal corpuscle and renal tubule. The renal corpuscle is the initial filtering component composed of an outer Bowman's capsule and inner glomerulus. It is followed by a long continuous tubular structure, called renal tubule. Depending on the relative positions to the renal corpuscle and the distinct ultrastructures, the renal tubule is further divided into several segments including the proximal tubule, loop of Henle, distal tubule and collecting tubule. Collecting tubules from different nephrons undergo a series of convergence to form collecting ducts and eventually connect to the ureter.

In mammals, the development of the kidney progresses through three stages: the pronephros stage, mesonephros stage and metanephros stage. The first two stages are transient; only the metanephros persists and eventually develops into a functional kidney. Therefore, renal development usually refers to the metanephric kidney formation.

In mice, metanephric kidney development begins around E11, and is initiated by the invasion of the ureteric bud into the metanephric mesenchyme.

Both components are derived from the intermediate mesoderm. Upon invasion, the ureteric bud and metanephric mesenchyme undergo a process of reciprocal induction (refer to Figure 1.6). The ureteric buds are induced by mesenchymal cells to branch and elongate; concurrently, the mesenchymal cells are induced by ureteric buds to aggregate, proliferate, and epithelialize, eventually forming nephrons. New nephrons are always induced in the outer layer of the cortex, and move to the inner cortex during maturation. This process persists until a few days after birth.

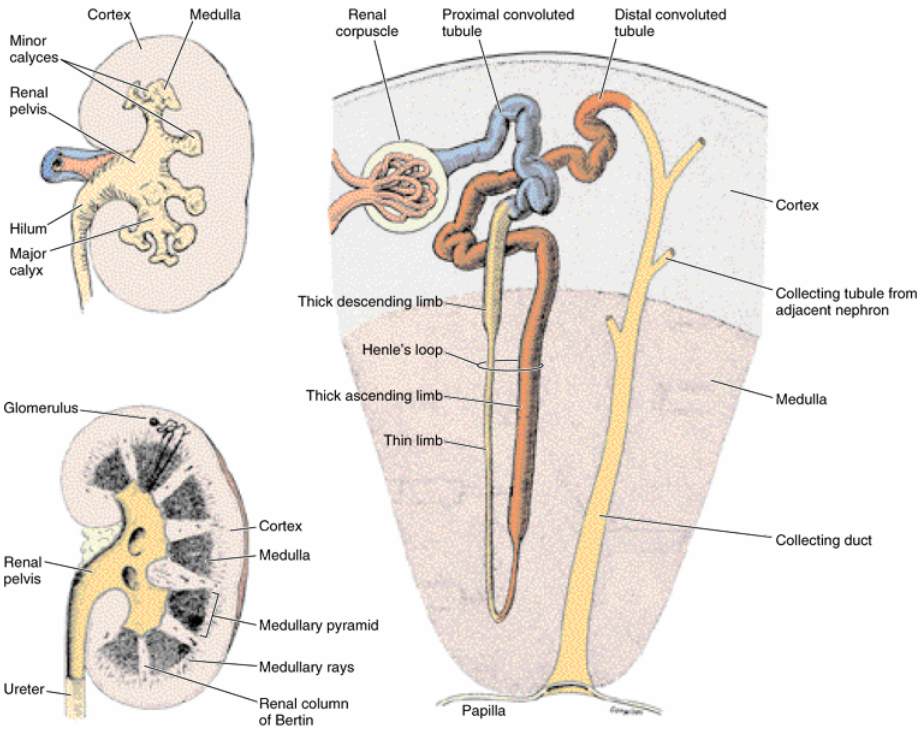

Figure 1.5 Kidney structure and nephron. (Adapted from Basic Histology by Luiz Carlos Junqueira & Jose Carneiro, tenth edition)

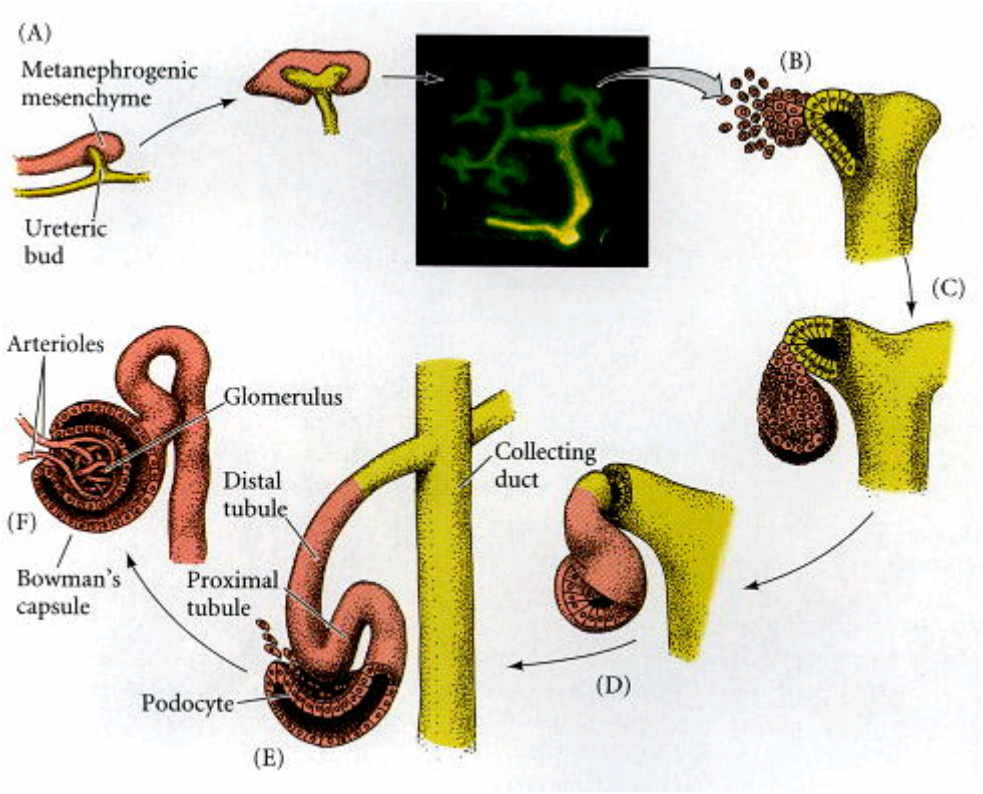

Figure 1.6 Nephrogenesis is a process of reciprocal induction between the ureteric bud and the metanephoric mesenchyme. (Adapted from Developmental Biology by Scott Filbert, 6th version)

Polycystic kidney disease (PKD)

Polycystic kidney disease (PKD) is a genetic disorder characterized by the presence of numerous cysts in the kidney. There are two major forms of PKDs depending on the patterns of inheritance: autosomal dominant PKD (ADPKD) and autosomal recessive PKD (ARPKD). In contrast to the rare incidence of ARPKD, ADPKD is one of the most common human renal diseases, affecting about 1 in 500-1000 humans (Igarashi and Somlo, 2002).

The pathogenesis of ADPKD has been genetically linked to mutations of two genes: PKD1 and PKD2 (1994; 1995; Mochizuki et al., 1996). Individuals with mutations of either PKD1 or PKD2 are predisposed to develop polycystic kidneys both in humans and mice. The protein products of these two genes are Polycystin-1 and Polycystin-2, respectively. Both proteins are recognized as transmembrane proteins by structure, which is consistent with their membrane-associated cellular distribution. Many proteins and pathways have been proposed to be regulated by polycystin proteins (Igarashi and Somlo, 2002; Torres and Harris, 2006; Wilson, 2004). However, despite many hypotheses, little is known about the function of these two proteins, which has prevented the development of successful treatments of PKD besides dialysis and kidney transplantation. The most recent studies suggested that these two proteins possibly function together as mechanoreceptors in the primary cilium, sensing the fluid-flow in the lumen and

regulating the Ca^{+} influx (Nauli et al., 2003). Still, the downstream signaling of polycystin-1 and polycystin-2 that mediates PKD needs to be further evaluated.

Role of mTOR signaling in PKD

Loss of function of either TSC1 or TSC2 in humans or mice results in the development of renal problems. Renal cyst is a common renal abnormality observed in the TSC patients. However, unlike PKD, renal cysts in the TSC patients appear limited in size and number and are usually harmless to normal renal function, although they do have the potential to develop further into cystadenoma and cystcarcinoma. Whether the cystogenesis in TSC and PKD shares a similar mechanism is not known, however, a small percentage (~2%) of TSC patients is associated with severe infantile PKD (Sampson et al., 1997). This is explained by the fact that the TSC2 gene is in close proximity to the PKD1 gene on chromosome 16 with only a 60-bp distance. Clinically, severe infantile PKD cases are usually associated with deletions on chromosome 16 that affect both genes (Brook-Carter et al., 1994; Sampson et al., 1997).

The first evidence that suggests TSC2 might be functionally involved in PKD is from the study of the Eker rat, a naturally occurring rat with inactivation of one TSC2 allele, which predisposes it to lose another TSC2 allele and makes it an useful animal model for studying TSC2 associated diseases (Kobayashi et al., 1995). Renal cysts are very common in adult Eker rats, while Kleymenova *et al.*

first noticed a few cases of Eker rats with severe PKD (Kleymenova et al., 2001). Further study on the cell line isolated from the cyst-lining cells suggested the loss of another TSC2 allele but intact PKD1 gene. However, the membrane localization of Polycystin-1 is missing in those cells, indicating TSC2 dependent cellular localization of Polycystin-1. Recently, Weimbs's group reported the finding of elevated mTOR activity in the cyst-lining cells of human and mouse PKD samples (Shillingford et al., 2006). More interestingly, they further demonstrated that application of the mTOR specific inhibitor, rapamycin, was able to effectively control cyst development in *Pkd1* conditional knockout mice. Based on this, they propose that mTOR activity is regulated by Polycystin-1 and is critical for cystogenesis. Furthermore, it has been reported that loss of BDH, a potential upstream regulator of mTOR, in renal tubule cells resulted in over activation of mTOR and polycystic kidneys in mice (Baba et al., 2008). All these results together indicate that dysregulation of TSC/mTOR might be involved in PKD, but still, the big question is how it is involved.

Chapter II Materials and methods

Mice breeding:

Pten^{loxP} mice (Suzuki et al., 2001) were a gift from Dr. Tak Mak (University of Toronto). *Nse-cre* line was generated in Dr. Suzanne J. Baker's lab (St. Jude Children's Research Hospital, Memphis) and characterized in our lab (Kwon et al., 2006b). *Tsc1*^{loxP} mice were a gift from Dr. David Kwiatkowski (Harvard Medical School, Boston). *Pten* mutant mice (*Nse-cre*; *Pten*$^{loxP/loxP}$) were generated by breeding between male *Pten*$^{loxP/loxP}$ mice and female *Nse-cre*; *Pten*$^{loxP/+}$ mice. Littermate controls used here were either with absence of *Nse-cre* or in a few cases *Nse-cre*; *Pten*$^{loxP/+}$. *Tsc1* mutant mice (*Nse-cre*; *Tsc1*$^{loxP/loxP}$) were generated by the similar strategy. Double mutant mice (*Nse-cre*; *Pten*$^{loxP/loxP}$ *;* *Tsc1*$^{loxP/loxP}$) were generated by crossing male *Pten*$^{loxP/loxP;}$ *Tsc1*$^{loxP/loxP}$ mouse with female *Nse-cre*; *Pten*$^{loxP/+}$ *; Tsc1*$^{loxP/+}$ mouse. In some cases, *cre* expression in wild type mice or in mutants (either *Pten* mutants or *Tsc1* mutants) was examined by using either the *Rosa-stop-lacZ* or *Rosa-stop-yfp* reporter mouse line (Soriano, 1999; Srinivas et al., 2001). *Pten* mutant mice in *C57/BL6* inbred background were used in the study described in chapter III, while mice in mixed background were used in the study described in chapter IV. All mouse protocols were approved by the Institutional Animal Care and Research Advisory Committee at University of Texas Southwestern Medical Center.

Rapamycin injection

Rapamycin powder (Sirolimus, LC Laboratories, Woburn, MA) was dissolved in ethanol and stored at a stock concentration of 25 mg/ml in aliquots at -20^{o}C. Working solution was prepared freshly before use with a final concentration of 1 mg/ml rapamycin (for the brain study) or 0.1 mg/ml rapamycin (for the kidney study) in 4% ethanol, 5% Tween 80 and 5% PEG400 (Kwon et al., 2003). For the brain study, mice were injected intraperitoneally (i.p.) with either rapamycin (10 mg/kg body weight) or vehicle once per day and five consecutive days per week (Monday to Friday); for the kidney study, mice were also i.p. injected, but delivered weekly with 2 mg/kg of rapamycin.

BUN measurement:

The whole blood of mice was collected and kept at RT for 30-45 min. before centrifuge. Serum was isolated by spinning the whole blood samples at 4000g for 3 min. Serum samples were then submitted to the mouse metabolic phenotyping core for BUN measurement (U.T. Southwestern Medical Center).

Histology and immunohistochemistry:

Mice were anesthetized with ketamine/xylazine (9:1 ratio) and then intracardially perfused with ice-cold PBS followed by 4% PFA. Brains and

kidneys were dissected out immediately after perfusion and kept in 4% PFA at 4^{o}C for further use.

For preparing paraffin sections, brains or kidneys were processed and embedded in paraffin. Tissues were sectioned sagittally at 5 μm thickness. For preparing vibratome floating sections, tissues were embedded in 3% agarose and cut coronally at 50 μm thickness. For preparing cryostat sections, tissues were first protected in 30% (w/v) sucrose in PBS for 2-3 days, which were then embedded in O.C.T. and sectioned at 6 μm thickness.

Usually sections with comparable anatomy were chosen from controls and mutants. Antibodies used for IHC were listed in table 2.1.

For DAB staining on paraffin sections, we used microwave antigen retrieval for all antibodies. We visualized primary antibodies by treating sections with biotinylated secondary antibody and followed by amplification with the peroxidase-conjugated avidin and DAB substrate (Vector Labs, Burlingame, CA). DAB-stained sections were counter-stained with hematoxylin.

For immunofluorescent staining on paraffin, vibratome or cryostat sections, we detected primary antibodies by secondary antibodies conjugated with Cy3 or Cy2 (Jackson Immunoresearch, West Grove, PA). Nuclei were stained with DAPI.

Table 2.1 Antibodies used for immunohistochemistry.

Antibody	Vender	Source
Pten	Cell Signaling	Rabbit
P-Akt (Ser473)	Cell Signaling	Rabbit
Akt	Cell Signaling	Rabbit
P-4E-BP1 (Thr37/46)	Cell Signaling	Rabbit
4EBP	Cell Signaling	Rabbit
P-S6 (Ser235/236)	Cell Signaling	Rabbit
S6	Cell Signaling	Mouse
Synapsin I	Chemicon	Rabbit
Calbindin	Swant	Mouse
Biotinylated LTL	Vector Lab	
GFP	Aves labs	Chicken
GFP	Molecular probes	Rabbit
BrdU	Dako	Mouse
BrdU	abcam	Rat

Western blotting

Mice were sacrificed by CO_2 inhalation. Kidneys or brain tissues (hippocampus and cortex) were dissected freshly and snap frozen in liquid nitrogen. To prepare the lysate, frozen tissues were homogenized in the lysis buffer containing 20 mM Tris-HCl , 150 mM NaCl, 1 mM EDTA, 1 mM EGTA, 1% TritonX-100, proteinase inhibitor (Roche, Mannheim, Germany), Ser/Thr phosphatase inhibitor and Tyr phosphatase inhibitor (Upstate, Temecula, CA). The homogenate was centrifuged at 14,000 rpm for 30 min. and supernatant was collected. Protein concentration was determined by using BCA kit (Pierce, Rockford, IL). 20 or 50 μg of each sample was loaded onto SDS-PAGE gel. Antibodies used for Western blotting were against PTEN, P-AKT-Ser473, AKT, P-4E-BP1 (Thr37/46), 4E-BP, P-S6 (Ser235/236), S6 (Cell Signaling, Beverly, MA), β-tublin or β-actin (Sigma, St. Louis, MO). Signal was developed by ChemiGlow West reagent (Alpha Innotech, San Leandro, CA) and visualized by Kodak Image Station 2000R (Rochester, NY).

X-gal staining:

To collect tissues for X-gal staining, embryos were collected freshly after sacrificing the mother with CO_2 inhalation and then fixed with 2% PFA overnight; postnatal mice were perfused with PBS followed by 2% PFA, and then the brain or kidney were dissected out and post-fixed in 2% PFA overnight.

For the brain study, 50 μm vibratome sections were used. For the kidney study, embryos or kidneys were cryo-protected with sucrose and sectioned at 12-μm thickness. The staining was performed as described previously with sections incubating in X-gal staining solution at 37^{o}C from 4 hours to overnight (Kwon et al., 2006b).

Golgi staining

We performed Golgi staining, image analysis including quantification of dendritic caliber and spine density as described previously (Luikart et al., 2005). Briefly, mice were perfused with PBS only. After dissection, whole brain was incubated in the Golgi staining solution (containing 1.25% potassium dichromate, 1.25% mercuric chloride and 1% potassium chromate) in the dark at RT for 10-12 days, followed by vibratome sectioning at 100 μm thickness. The staining was visualized by developing sections in ammonium hydroxide and then a fixer solution (Kodak, Rochester NY).

Timm's staining

For Timm's staining, mice were perfused with ice-cold 0.37% (w/v) sodium sulfide followed by 4% PFA. We dissected out the brain, post-fixed in 4% PFA overnight and cryo-protected in 30% sucrose for 2–3 days. 16-μm-thick

coronal sections were prepared and then a modified Timm's staining was performed as described previously (Danscher et al., 2004).

Measurements

All measurements were performed using MetaMorph software (Universal Imaging Corporation, West Chester, PA). We measured nuclear diameter of dentate granule neurons as an indication of soma size (Kwon et al., 2003). To estimate the thickness of the mossy fiber tract, we measured the wideness of the out-coming axonal bundles from the dentate gyrus that were double-labeled with Synapsin I and Calbindin. To assess dendritic size, we measured the length of Calbindin-stained neuronal processes into the ML. Data were analyzed with ANOVA, followed by post hoc Student's *t*-test.

Behavioral tests

Mutant mice were studied along with littermate controls in four groups: vehicle-treated controls, vehicle-treated *Pten* mutant mice, rapamycin-treated controls and rapamycin-treated *Pten* mutant mice. Behavioral tests were performed as described previously (Kwon et al., 2006a). The open field test was performed for 10 min in a brightly lit, 48 X 48 cm^2 white plastic arena with a center zone defined as a 15 X 15 cm^2 square. Time spent in the center zone and total travel distance were recorded using videotracking software (Noldus). The

social interaction tests were performed in a neutral cage in the dark under red light by pairing a test mouse with a male juvenile mouse. During a 2 min time window, the time that the testing mouse actively approached and sniffed the social target was recorded. After this initial interaction, the test was repeated after 3 days by re-introducing the same social target. Above behavioral tests were performed blindly to genotype and treatment.

EEG/EMG recording

For EEG/EMG analysis, *Pten* mutant (n = 12) and wild-type mice (n=3) were anesthetized and surgically implanted for long-term EEG/EMG monitoring as described previously (Chemelli et al., 1999). The design for the EEG/EMG implant allowed precise insertion of electrodes, targeting the frontal and occipital cortices at a consistent depth that just touches the dura and minimizes surgical trauma. Mice were housed individually under a 12 hr light:dark cycle at 25°C (lights-on: CT 0000), with food and water being replenished as necessary at CT 1200 each day, but they were not otherwise disturbed. Mice were habituated to the recording conditions for 2 weeks before baseline EEG/EMG signals were recorded over a period of 3 days, beginning at lights-off (CT 1200). In the following week, the mice were divided into two groups: a rapamycin-treated group (n = 6 mutants, n = 3 controls) and a vehicle-treated group (n = 6 mutants). Each week, the animals were i.p. injected with either rapamycin or vehicle once

per day between 10:00 and 11:00 am for 5 successive days. The EEG/EMG was recorded from the second day of the injection continuing for 3 days, and this procedure was repeated for 4 weeks to evaluate the chronic effect of the drug. No adverse effects from the injection were observed in either group, and the bodyweights remained stable throughout the study. Subsequently, the EEG/EMG record was visually screened for seizure epochs. Seizures were characterized as a spike-wave pattern on the EEG, typically accompanied by atonic periods or sustained rhythmic contractions on the EMG. Each seizure lasting for 2 sec or more was noted. The total number of seizures during the 12 hr dark and light periods was analyzed, as well as the time of occurrence and the duration of each seizure. One-way ANOVA with Bonferroni's multiple comparison as a post-hoc test was applied to analyze differences within groups.

Chapter III: Pharmacological inhibition of mTOR suppresses anatomical, cellular and behavioral deficiencies in neural specific *Pten* knockout mice.

Background:

Previously, we generated *Nse-cre;Pten*$^{loxP/loxP}$ mice (*Pten* mutant mice hereafter) with *Pten* ablation in subsets of post-mitotic neurons in cortex and hippocampus. We demonstrated those *Pten* mutant mice develop macrocephaly and additional behavioral abnormalities reminiscent of human autism, including reduced social activity, increased anxiety, and sporadic seizures (Kwon et al., 2006a; Ogawa et al., 2007). At the cellular level, we observed two major morphological changes after *in vivo* loss of *Pten*: loss of neuronal polarity and neuronal hypertrophy. The latter is characterized not only by enlarged somata, but also increased dendritic size and thickness of the axon bundle. This is consistent with *in vitro* studies of PI3K/AKT pathway activation (Jaworski et al., 2005; Kumar et al., 2005).

However, a lingering question is which AKT downstream pathway is responsible for these cellular and behavioral changes. Among the various PI3K/AKT downstream pathways, TSC/mTOR becomes a very attractive

candidate. First, mutations of either the TSC1 or TSC2 gene cause tuberous sclerosis in humans, and about 25-50% of these patients show autistic syndrome (Smalley, 1998; Smalley et al., 1992; Wiznitzer, 2004). Second, it has been demonstrated that loss of *Tsc1* results in neuronal hypertrophy both *in vitro* and *in vivo* (Jaworski et al., 2005; Meikle et al., 2007; Tavazoie et al., 2005).

In the current study, we examined the role of the TSC/mTOR pathway on the cellular and behavioral changes of the *Pten* mutant mice through the use of a specific mTOR inhibitor, rapamycin. Our results indicate a major contribution of this pathway to the abnormal cellular morphology phenotype. Further, attenuation of the mTOR pathway in *Pten* mutants by rapamycin treatment has surprising consequences on neuronal hypertrophy, seizures, and social behavior. Finally, we provide additional genetic data to support the importance of the TSC/mTOR pathway in the observed phenotypes. Conditional ablation of TSC1 using the same *Nse-cre* transgenic mouse line mimics the morphological features observed with the *Pten* mutant mice. These data point to a common signal transduction pathway and to confined neuroanatomical regions (cortex and hippocampus) that are potentially responsible for the autism-like symptoms observed in individuals with *TSC* and *PTEN* mutantions.

Results:

Rapamycin effectively blocks mTOR signaling in the CNS

We performed a dose-response experiment to determine an effective rapamycin dose that would inhibit mTOR activity in mouse cortex and hippocampus. Rapamycin (Sirolimus) (Heitman et al., 1991) was administered for five consecutive days at doses of 0, 10, 20, and 40 mg/kg. At all concentrations tested, the mice showed no adverse health reactions and maintained normal weight. Mice were sacrificed on the last day of injection for analysis. As readout for mTOR activity, we assayed levels of phospho-Ser235/236-S6 (P-S6, hereafter) and determined that 10 mg/kg of rapamycin effectively reduced mTOR signaling in both the hippocampus and cortex (Figure 3.1A).

As demonstrated previously, loss of *Pten* causes activation of mTOR signaling in the cortex and hippocampus (Kwon et al., 2006a). Thus, we assessed the ability of 10mg/kg of rapamycin to attenuate mTOR signaling in *Pten* mutant brains. As illustrated in Fig. 3.1B and C, this dose of rapamycin administered over 5 days was sufficient to attenuate S6 phosphorylation to wild type control levels. We therefore adopted this rapamycin dosage in all subsequent studies.

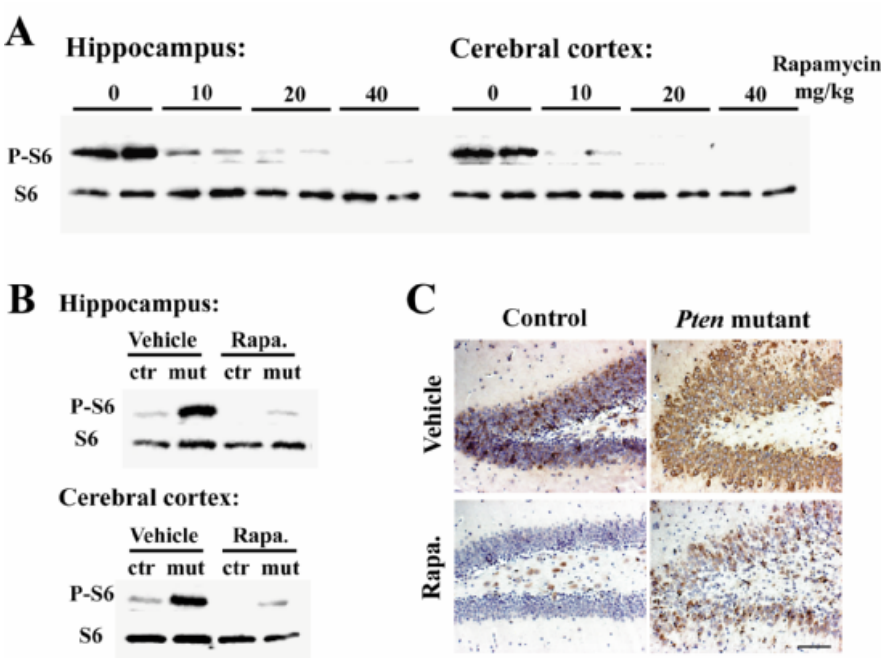

Figure 3.1 Rapamycin effectively blocks mTOR signaling in the brain. (A) Dose-dependent suppression of P-S6 in cortex and hippocampus by rapamycin injection. Rapamycin was given to two-month-old wild-type mice daily for 5 days. (B-C) 10 mg/kg rapamycin effectively reduced P-S6 in both hippocampus and cortex of *Pten* mutant mice, as shown by Western blotting (B) and IHC (C) Control and mutant mice at ten weeks of age were injected with either vehicle or 10 mg/kg rapamycin daily for 5 days. Scale bar, 100 μm.

Rapamycin can prevent or reverse macrocephaly in Pten mutant mice.

In our mouse model, deletion of *Pten* is mainly restricted to subsets of post-mitotic neurons in the cortex and hippocampus (Kwon et al., 2006b). Minimal *cre* activity could be detected at P0, and robust activity only became apparent after two weeks of age (Figure 3.2). Maximal *cre* activity was achieved at four weeks,as visualized with *Rosa26-stop-lacZ* cre reporter mice (Soriano, 1999).

Loss of *PTEN* in the brain results in macrocephaly in human and mouse (Backman et al., 2001; Groszer et al., 2001; Kwon et al., 2001; Marsh et al., 1999). The brain weight of *Pten* mutant mice has been carefully monitored and shown to progressively develop into macrocephaly that is detectable as early as four to five weeks of age, reaching statistical significance at two months of age (Kwon et al., 2006a). This timing correlates with the appearance of abnormal behavior, which begins at five to six weeks of age and is fully penetrant at two to three months of age. We chose to administer rapamycin to two cohorts of mutant and control mice: a presymptomatic young group (5-6 weeks old) and a symptomatic adult group (10-12 weeks old). Thus, in the former group, rapamycin activity would be present at the earliest manifestation of abnormality and would be tested for prevention of symptoms. In the latter group, rapamycin delivery commenced when symptoms were fully penetrant to test the potential for reversal. For each

group, mutants and age-comparable controls were injected with either vehicle or 10mg/kg rapamycin daily. Mice were sacrificed after either four or six weeks of drug treatment for analysis as shown in Figure 3.3A.

Overall, the mice appeared healthy during rapamycin administration, although slight growth effects were observed after long-term treatment. In the young group, rapamycin-injected mice showed a 5-9% reduction in body weight compared to vehicle-injected controls. This effect was less obvious in the adult group, which shared a similar trend but did not reach statistical significance. To account for the overall effect of rapamycin on growth, brain/body weight ratio was used to assess relative brain size (Figure 3.3B). In the young group by the fourth week of injection, the vehicle-treated mutant mice (9-10 weeks old) already showed significantly increased brain/body weight ratio compared to control mice. In contrast, the mutants receiving rapamycin showed normal brain/body weight ratio. In the adult group, the same effect was observed. In the vehicle-treated group, the macrocephaly (17% increase in brain weight) was more dramatic than in the young group (7% increase in brain weight), yet rapamycin effectively reversed brain weight to wild type levels (Fig. 3.3B). As previously described, the enlarged brain size is mainly the consequence of *Pten* null cell-autonomous overgrowth in the two brain regions where *cre* activity is confined (cortex and hippocampus). Consistent with the brain weight data, the enlargement of cortex

and hippocampus in mutants is controlled by rapamycin, as shown by Nissl staining of the treated young group of mice (Figure 3.3C).

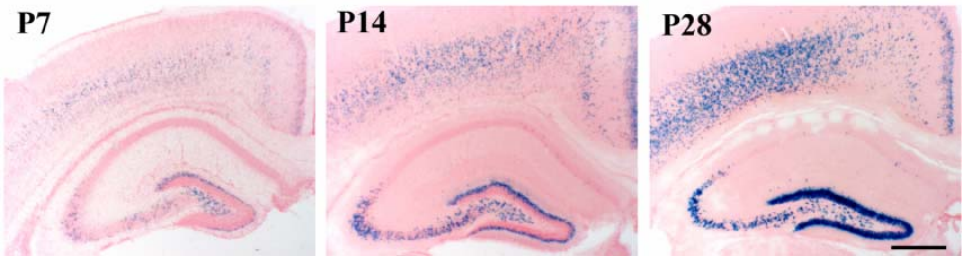

Figure 3.2 *Nse-cre* activity increased progressively during brain development. Data shows that cre expression increases gradually after birth and becomes fully activated after P28. Cre activity was detected by crossing with *Rosa26-stop-lacZ* reporter mice. Scale bar, 500μm.

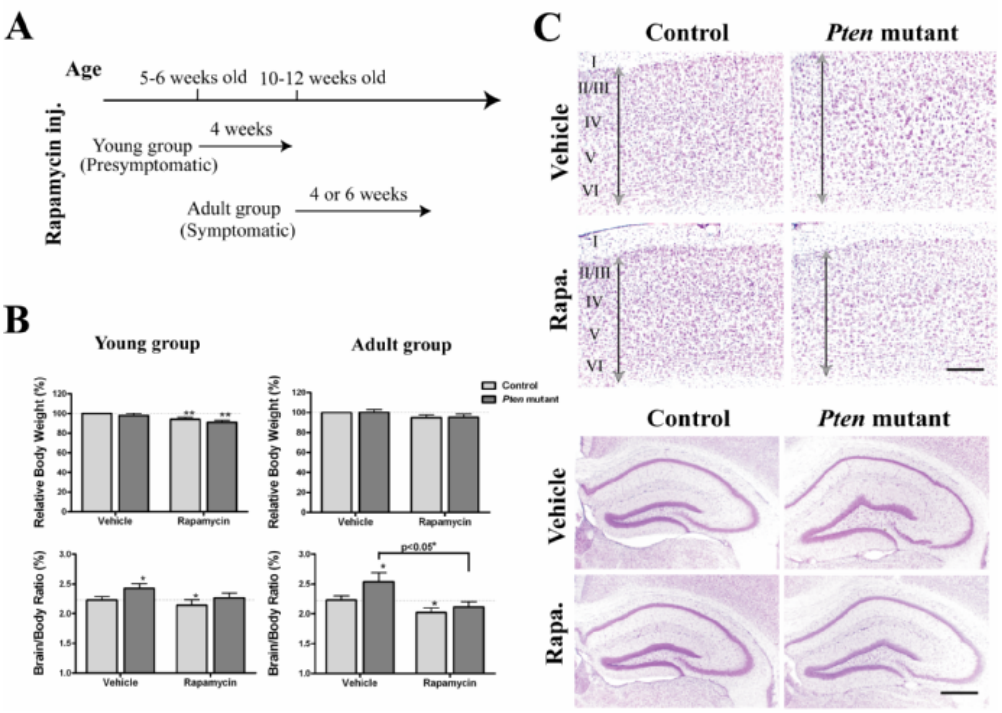

Figure 3.3 Rapamycin can prevent or reverse macrocephaly in *Pten* mutant mice. (A) Rapamycin injection strategy. Rapamycin was applied to two cohorts of mice at different ages: a young group (5-6 weeks old) and an adult group (10-12 weeks old). Mutants and controls injected with either vehicle or 10 mg/kg rapamycin were analyzed after 4 or 6 weeks of daily injections. (B) Rapamycin prevents or reverses the brain enlargement of *Pten* mutant mice. The effect of rapamycin on brain and body weight was measured after 4 weeks for the young group or after 6 weeks for the adult group (n=15 mice per group for body weight

measurement, n=8 mice per group for brain/body ratio). Data are mean ± SEM and analyzed by paired *t*-test. *p<0.05 and **p<0.01, as compared to control mice treated with vehicle or between groups as indicated. (C) Representative Nissl staining shows that rapamycin treatment suppressed the enlargement of cortex (top panels, scale bar, 200 μm) and hippocampus (bottom panels, scale bar, 500 μm) when applied to young *Pten* mutant mice for 4 weeks. Arrows show thickness of cortical layers II to VI.

Rapamycin suppresses hippocampal granule cell hypertrophy.

We have assessed the changes in cell morphology caused by *Pten* loss using various techniques and demonstrated that brain enlargement is not only due to the enlarged soma size, but also the result of neuronal process hypertrophy, including increased dendritic size and thickened axon bundles (Kwon et al., 2006a). We therefore first examined the effect of rapamycin on neuronal hypertrophy in the presymptomatic group of mice.

On tissue sections, the cellular boundary of granule cells in the dentate gyrus is not clearly identifiable because the nuclei of granule neurons are prominent and surrounded by a thin layer of cytosol. We therefore used nuclear diameter to reflect soma size (Kwon et al., 2006a; Kwon et al., 2003). PTEN immunostaining clearly illustrates that *Pten* negative cells (blue cells, hematoxylin counterstained) are obviously larger than *Pten* positive cells (brown cells), but the soma hypertrophy does not develop in mutant mice undergoing rapamycin treatment (Figure 3.4 A & B). To examine the effect of the drug on neuronal processes, we again took advantage of the well-established circuitry in the hippocampus. The granule cells of the dentate gyrus spread their dendrites out towards the molecular layer (ML), while the axons form the mossy fiber tract that projects through the polymorphic layer to synapse onto the CA3 region. The mossy fiber tract axonal bundle was visualized by immunohistochemistry (IHC)

using antibodies to Synapsin I, a presynaptic marker, and to Calbindin, which is expressed in both soma and processes. The increased thickness of the mossy fiber tract seen in vehicle-treated mutants was dramatically suppressed by rapamycin administration (Figure 3.5A&B). This result was confirmed by Timm's staining, which specifically highlights the mossy fiber tract (Figure 3.5 C). Dendritic growth was measured by the thickness of the ML, defined here as the length of Calbindin-stained neuronal processes into the ML. The data indicated that dendritic overgrowth was also reduced by rapamycin (Figure 3.5 A& D).

We further observed that, at the end of treatment, four of eight mutants treated with vehicle exhibited ectopic Synapsin I reactivity in the inner ML (Figure 3.5 A, arrowheads), reflecting loss of polarity in granule neurons. This is a common feature of older mutant mice (Kwon et al., 2006a). Interestingly, none of the six rapamycin treated mutants showed ectopic Synapsin I. Similar results were obtained with Timm's staining, with two of five mutants treated with vehicle showing ectopic staining in the inner ML but none of the four mutants treated with rapamycin. Taken together, these data indicate that, when administered early in presymptomatic mice, rapamycin can suppress the development of neuronal process hypertrophy and the loss of neuronal polarity caused by *Pten* ablation.

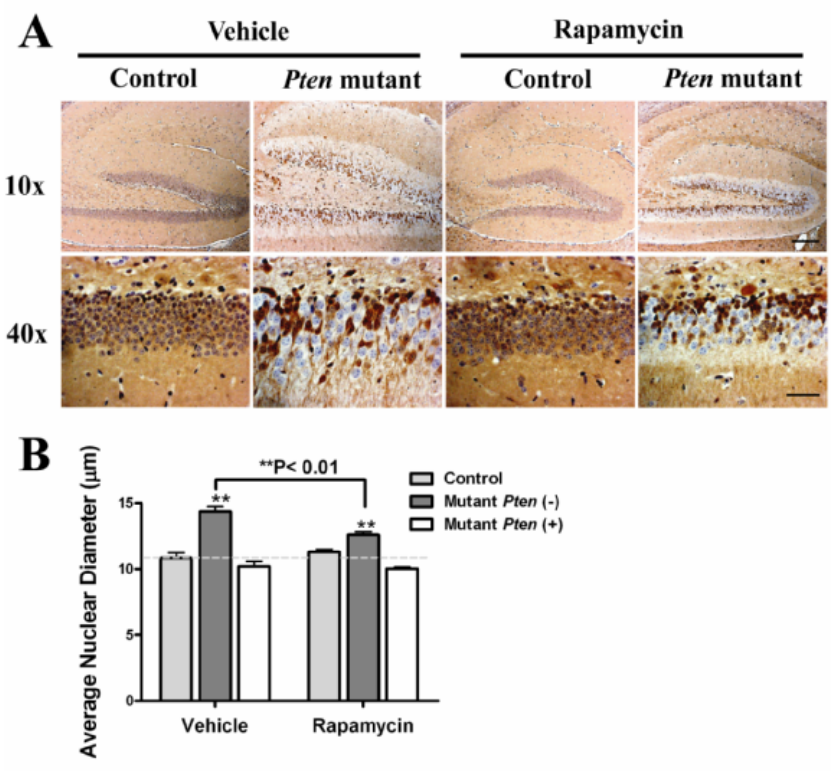

Figure 3.4 Rapamycin suppresses soma hypertrophy of dentate granule cells in young *Pten* mutant mice. (A) PTEN immunostaining on dentate granule cells. In *Pten* mutant mice, *Pten* negative cells (mutant *Pten* (-), blue cells) are distinguishable from *Pten* positive cells (mutant *Pten* (+), brown cells). Scale bars, 200 μm for upper panels and 50 μm for lower panels. (B) Quantification reveals a significant suppression of soma hypertrophy of *Pten* negative neurons after rapamycin treatment. n=4 animals per group. Data are mean ± SEM and analyzed by ANOVA, followed by post hoc *t*-test. *p<0.05 and **p<0.01, as compared to control mice treated with vehicle or between groups as indicated.

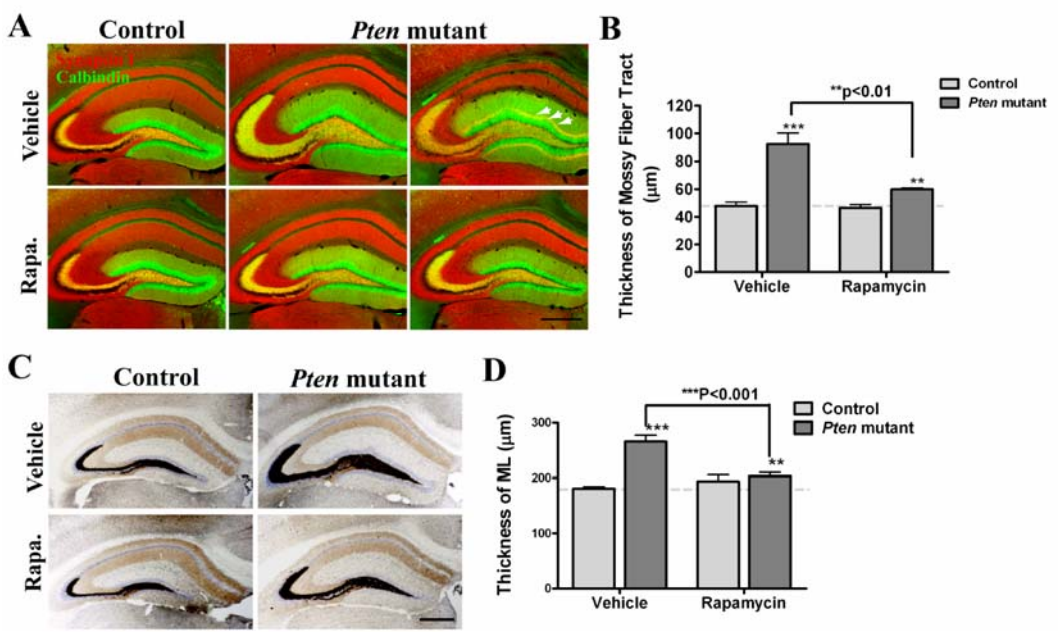

Figure 3.5. Rapamycin inhibits dendritic and axonal hypertrophy of dentate granule cells in young *Pten* mutant mice. (A) Immunostaining on 50-μm floating sections for Synapsin I (red) and Calbindin (green) shows reduced dendritic and axonal hypertrophy in *Pten* mutants after rapamycin treatment. Ectopic Synapsin I staining (arrowhead) in the inner molecular layer were observed in some vehicle treated *Pten* mutants. Scale bar, 500 μm. (B) Quantification reveals that increased thickness of mossy fiber tract in *Pten* mutant mice was significantly reduced after rapamycin treatment. The thickness of mossy

fiber tract is defined by the width of the axon bundle that coming out of the dentate gyrus in Synapsin I and Calbindin double-stained sections. n=8 mice for vehicle treated groups; n=6 mice for rapamycin-treated groups. (C) Timm's staining to visualize mossy fiber tract. n=4 or 5 mice were examined per group. Scale bar, 500μm. (D) Increased thickness of the molecular layer in *Pten* mutant mice was significantly reduced after rapamycin treatment. Data are mean ± SEM and analyzed by ANOVA, followed by post hoc *t*-test. *$p<0.05$, **$p<0.01$ and ***$p<0.001$, as compared to control mice treated with vehicle or between groups as indicated.

Rapamycin inhibits development of cortical neuron hypertrophy.

Another region affected in the *Pten* mutant mice is the cortex, where *cre* expression is restricted mainly to layers III to V with about 30-60% neurons showing *cre* activity. We examined pyramidal cells as an example of cortical neurons in the presymptomatic group of mice. Neuronal morphology was visualized by IHC with antibodies against SMI 311 and PTEN. SMI 311 is a pan-neuronal neurofilament antibody that detects a subset of pyramidal cells in cortical layers III and V (Ulfig et al., 1998). In mutant mice, most *Pten* null pyramidal cells, if not all, had obviously larger somata, and were often accompanied by brighter staining of SMI 311(Figure 3.6A, arrowhead). Similar phenomena have been reported for neurons that lack *Tsc1*, suggesting neuronal hypertrophy with increased expression of neurofilament (Meikle et al., 2007). Compared to controls, the mutant samples showed overall increased SMI 311 staining, with more detectable SMI 311 positive cells over the cortex and dramatically enhanced signal per cell (Figure 3.6B). In mutant mice treated with rapamycin, the overall SMI 311 signal remained qualitatively higher than that in control but the extent was reduced, as was the thickness of the dendritic caliber (Figure 3.6B, arrow). Taken together, the above data indicate a surprising effectiveness of rapamycin to impede development of neuronal abnormalities and hence the macrocephaly observed in *PTEN* mutant mice when the timing of treatment coincides with the earliest appearance of the phenotype.

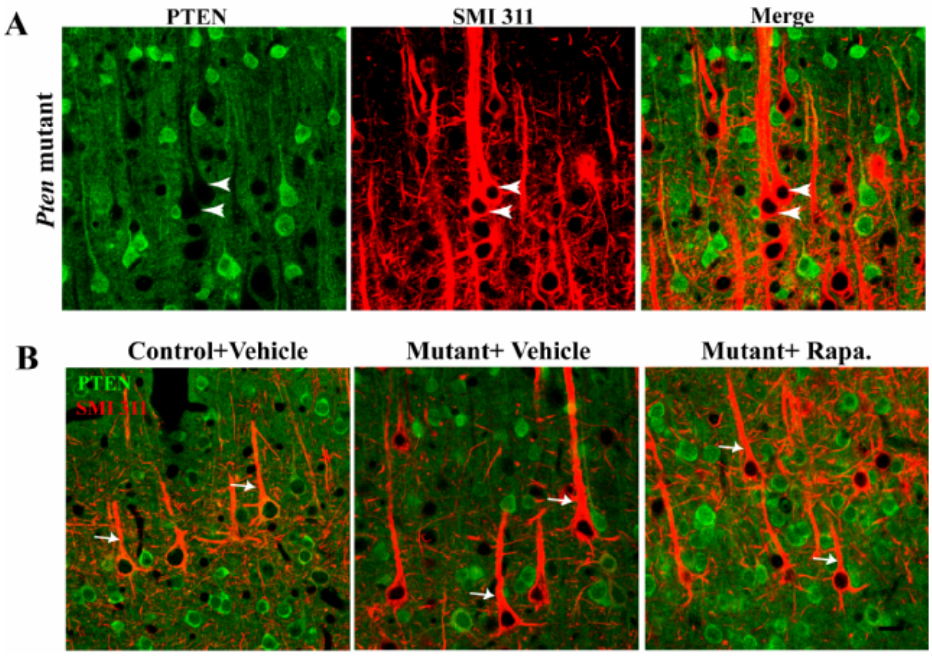

Figure 3.6. Rapamycin inhibits development of cortical neuron hypertrophy in young *Pten* mutant mice (A) Floating sections from *Pten* mutants were immunostained with PTEN (green) and SMI 311 (red). Arrowheads highlight *Pten*-null hypertrophic neurons with bright SMI 311 staining. (B) PTEN and SMI 311 double staining shows inhibition of dendritic hypertrophy by rapamycin treatment on *Pten*-null neurons. Arrows highlight the primary dendrites of SMI 311 positive neurons. Scale bar, 20 μm.

Rapamycin reverses dentate gyrus enlargement but not ectopic axonal projections.

Pten mutant mice develop neuronal abnormalities progressively. By 4 months of age the hippocampal dentate granule layer begins to show signs of abnormal foliation and compression of CA1 begins to show (Kwon et al., 2006a). To evaluate whether rapamycin could reverse already established morphological abnormalities, we treated a second cohort of mice beginning at 10-12 weeks of age (adult group) for four or six weeks. Our results indicate that, while not as effective as treating presymptomatic mice, rapamycin was able to significantly reverse several of the morphological abnormalities in older mice (Figure 3.7A). In contrast to the vehicle-treated mutant, the hippocampus of rapamycin-treated *Pten* mutants regained much of its structural integrity, although some compression of CA1 remained. However, in contrast to the younger cohort study, ectopic Synapsin I staining in the ML persisted in the drug-treated cohort even after 6 weeks of rapamycin treatment. These data indicate that the established granule cell loss of polarity could not be reversed. Nonetheless, the extent of the Synapsin I staining in the ML was reduced and mainly restricted to the inner ML (Figure 3.7A, arrowhead). The enlarged cell size of *Pten* null granule cells was also progressively reversed by rapamycin treatment (Figure 3.7B, 6C). In addition, the granule cell layer partially regained its tight organization, with less extracellular spaces that were probably previously occupied by the enlarged dendritic processes.

To further visualize individual cell morphology, we performed Golgi staining. As previously shown (Kwon et al., 2006a), granule cells in mutant mice are globally enlarged. After rapamycin treatment, dendritic size was reversed, accompanied by reduced dendritic caliber thickness and spine density (Figure 3.8). However, in both vehicle and rapamycin-treated samples, granule cells with multiple processes into polymorphic layers were occasionally observed, suggesting loss of polarity (Figure 3.8A, arrow head). This, together with Synapsin I staining result, suggested that rapamycin, when applied to older mice, could not inhibit the eventual loss of polarity.

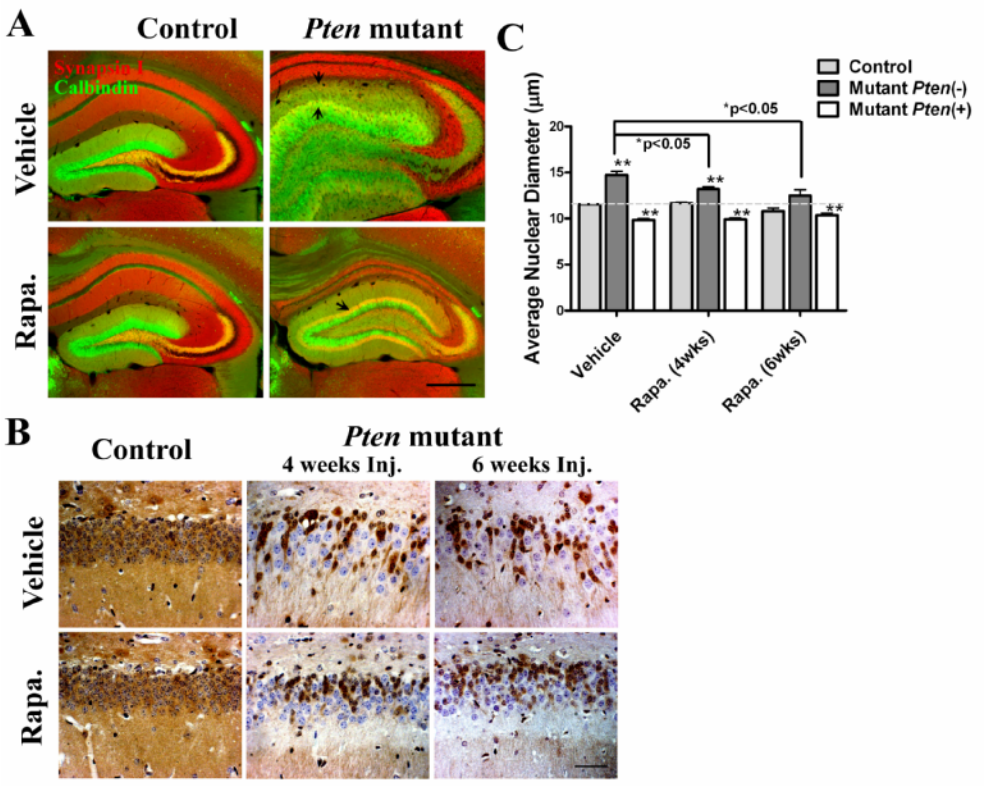

Figure 3.7. Rapamycin reverses dentate gyrus enlargement, but not ectopic axonal projections when applied to adult *Pten* mutant mice. (A) Immunostaining shows that rapamycin substantially reverses dentate gyrus hypertrophy, but axonal ectopia (arrows) still persist after six weeks of treatment in adult *Pten* mutant mice. Scale bar, 500 μm. (B) PTEN immunostaining on dentate granule cells demonstrates reversal of soma hypertrophy of *Pten* negative cells and restored granular layer organization after rapamycin treatment. Scale bar, 50 μm. (C) Quantification demonstrates the reversal of soma hypertrophy of *Pten*

negative cells. n=4 brains per group. *$p<0.05$ and **$p<0.01$, as compared to control mice treated with vehicle or between groups as indicated.

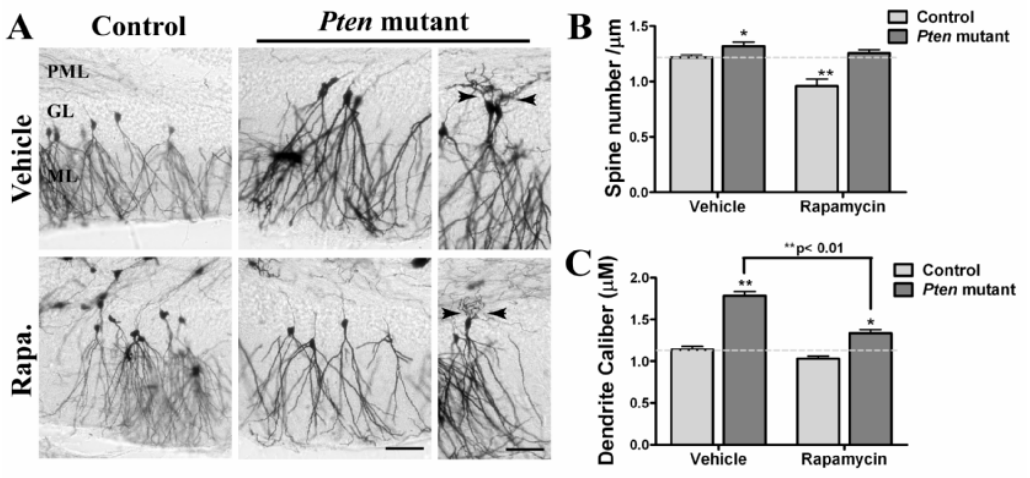

Figure 3.8 Golgi staining reveals reversal of neuronal hypertrophy, but not neuronal polarity by rapamycin in symptomatic mice. (A) Representative Golgi staining shows reversal of neuronal hypertrophy in the dentate gyrus of *Pten* mutant mice after 4 weeks of rapamycin treatment. PML, polymorphic layer. GL, granular layer. ML, molecular layer. Scale bar, 50μm. (B-C) Quantification shows that increases of spine density and dendritic caliber in *Pten* mutant mice were decreased after rapamycin treatment. n=3 brains were analyzed for each group. 5-10 primary dendritic branches were counted for each brain. Data are mean ± SEM and analyzed by ANOVA, followed by post hoc *t*-test. *p<0.05 and **p<0.01, as compared to control mice treated with vehicle or between groups as indicated.

Beneficial effects of rapamycin on behavior

We previously demonstrated that *Pten* mutant mice have increased anxiety and impaired social behavior in a series of experimental paradigms (Kwon et al., 2006a). We therefore tested whether rapamycin treatment in a young cohort could prevent development of these abnormal behaviors. Since at the cellular level the effects of rapamycin were gradual, we opted for the 4^{th} week of drug administration to examine the behaviors.

Consistent with our previous findings, in the open field test , vehicle-treated mutant mice spent significantly less time in the center of the open field compared to controls, indicating increased anxiety in the mutants (Figure 3.9A). Interestingly, after treatment with rapamycin, this difference was no longer apparent. A trend of increased time spent in the center was observed in mutant mice treated with rapamycin versus mutants treated with vehicle, suggesting rapamycin treatment reduced anxiety of *Pten* mutant mice. Mice were also examined in a test for reciprocal social interaction. As before, vehicle-treated mutants showed a significant decrease in social interaction compared to controls. Rapamycin treatment produced a clear increase in social interaction in the mutants. This effect of rapamycin on *Pten* mutant mice occurred in spite of its opposite effect on control mice (Figure 3.9B). This trend was also seen when mice were re-exposed to the same social target three days later. Thus, rapamycin

appears to specifically prevent development of anxiety and social behavioral abnormalities in *Pten* mutants when administered early.

Pten mutant mice also develop an age-related increase of spontaneous seizures (Ogawa et al., 2007). We therefore investigated whether rapamycin exposure would have an effect on seizures. As shown in Figure 3.10A, electroencephalogram/electromyogram (EEG/EMG) monitoring was performed over a period of five weeks for each mouse. Each week, EEG/EMG signals were recorded on three consecutive days (Tuesday to Thursday). For each mouse, baseline EEG/EMG was recorded at the first week. Then mutant mice were divided into two groups that were treated with either rapamycin or vehicle from starting at the second week. As anticipated, most mutant mice (n = 11) developed spontaneous seizures during the period of study, with the exception of one mouse in the drug-treated group that only displayed occasional epileptiform activity (e.g., spikes and spike-waves) but not full seizures. During the seizures, repetitive spike-wave patterns were noted, sometimes accompanied by rhythmic slow activity. Continuous spike-wave bursting was also seen. In the baseline EEG/EMG recording, though the severity of the seizures varied between individual animals, there was no significant difference in either frequency or duration of the seizures between vehicle and rapamycin-treated groups. However, compared to baseline, the mean duration of the seizures decreased significantly in

the drug-treated group in weeks 3 and 4 ($F[4,25]=3.172$, $p<0.05$), but not in the vehicle-treated group (Figure 3.10B). In addition, the tendency towards reduced seizure occurrence approached significance in the drug-treated group, despite large individual variance (Figure 3.10B). It is also worth mentioning that two mutant mice from the vehicle-treated group developed severe status epilepticus as the study progressed, resulting in premature death during the third week of treatment. Wild-type control mice ($n = 3$) treated with rapamycin did not develop seizures or display adverse effects.

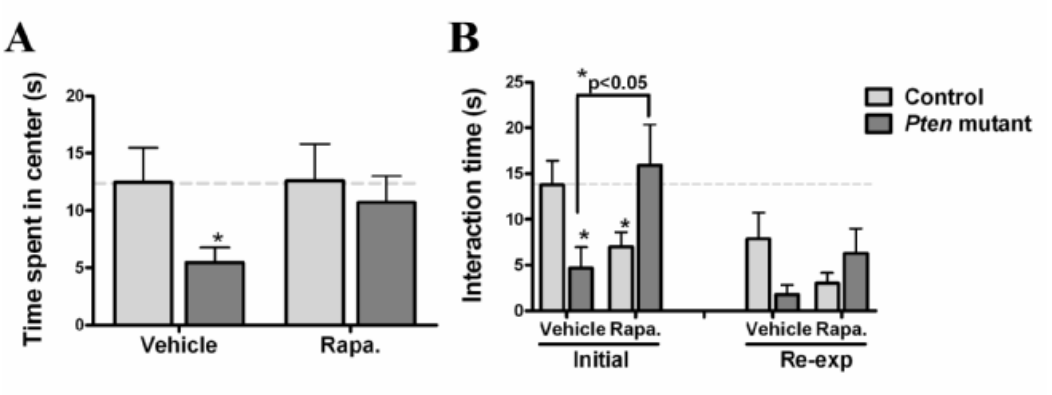

Figure 3.9 Rapamycin treatment reduces anxiety and improves social activity. A) In the open field test, rapamycin-treated *Pten* mutant mice show no significant difference from rapamycin-treated controls, whereas vehicle-treated *Pten* mutants show statistically significant decrease in center time compared to vehicle-treated control mice. (B) Rapamycin treatment increases social interaction time of *Pten* mutants and has the opposite effect on control mouse social interaction. n= 9 for vehicle-treated groups, n= 12 for rapamycin-treated control, and n=10 for rapamycin-treated *Pten* mutants. *$p<0.05$, as compared to control mice treated with vehicle or between groups as indicated.

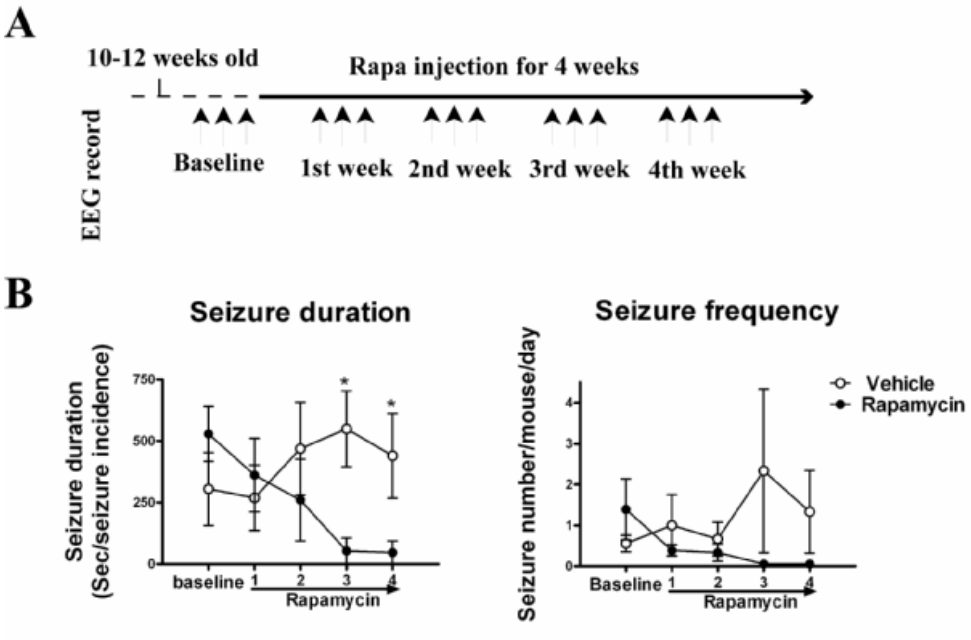

Figure 3.10 Rapamycin controls seizure frequency and duration (courtesy of Dr. Shiori Ogawa and Dr. Christopher Sinton). (A) Strategy of EEG/EMG monitoring. (B) Rapamycin injection progressively reduces seizure duration and frequency of *Pten* mutant mice. n=6 mice per group. *$p<0.05$, as compared between vehicle and rapamycin-treated mutants. Data are mean $\pm$ SEM and analyzed by ANOVA, followed by post hoc *t*-test.

Feedback effects on AKT

It has been suggested that chronic rapamycin exposure can have negative effects on AKT activity (Sarbassov et al., 2006; Sarbassov et al., 2005). Studies show that TOR complex 2 (TORC2) can effectively phosphorylate AKT at serine 473, which is important for AKT activity. Though only TOR complex 1 (TORC1) is rapamycin-sensitive, long-term rapamycin treatment can cause the depletion of mTOR from TORC2, thereby negatively affecting AKT activity as well. However, this feedback effect is context dependent, as *in vitro* not every cell line exposed to rapamycin results in downregulation of P-AKT-S473 level (Sarbassov et al., 2006). To examine potential chronic effects of rapamycin on AKT activity in our system, we collected cortical and hippocampal tissues at different post-injection points for Western blotting analysis of P-AKT-S473 levels. The data indicate that AKT-S473 phosphorylation is reduced by chronic rapamycin exposure in both treated controls and mutants (Figure 3.11A). The extent of inhibition is not progressive after one week of rapamycin exposure and remains relatively constant over a six week period (not shown). However, the overall P-AKT-S473 level in drug-treated mutants remained higher than that in vehicle-treated controls, as also supported by immunostaining of P-AKT-S473 on the dentate gyrus (Figure 3.11B). For each time point, we examined two sets of animals and a similar effect was observed in the cortex (data not shown). Therefore, we are unable to exclude the possibility that the effects of rapamycin on *Pten* mutant mice are in part

exerted through this feedback action of suppressing AKT activity and thus potentially implicating additional effectors downstream of AKT.

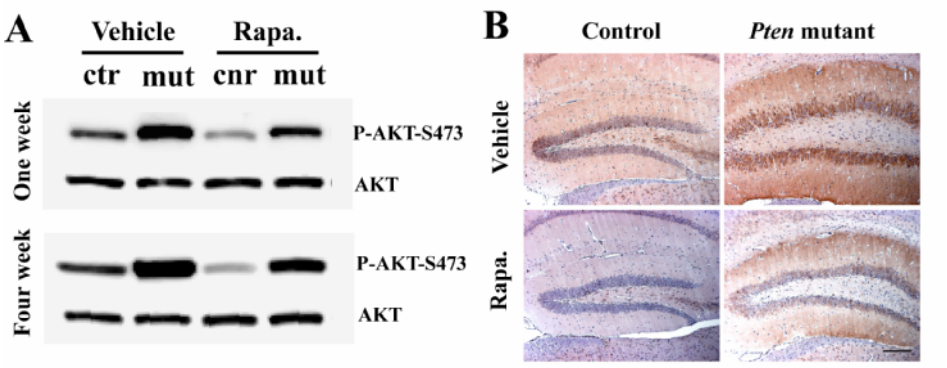

Figure 3.11. Long-term rapamycin treatment has a feedback effect on AKT activity. (A) Rapamycin treatment has a negative feedback effect on P-AKT-S473 level as shown by Western blotting on hippocampus. (B) Immunostaining of P-AKT-S473 on dentate gyrus of adult mice treated with either vehicle or rapamycin for four weeks. Scale bar, 200 μm.

TSC1 mediated neuronal hypertrophy in vivo

To further assess the role of the mTOR pathway on cell morphology *in vivo*, we crossed *Tsc1* conditional knockout mice (*Tsc1*^{loxp}) mice with the same *Nse-cre* line. Unexpectedly this cross resulted in reduced viability (data not shown). We examined three *Tsc1* mutants that survived to 10 weeks of age. Reminiscent of the *Pten* mutants, these mice appeared hyperactive and were prone to sporadic seizures (data not shown). Although the *Tsc1* conditional mutants examined were approximately 20% smaller than their littermate controls, they showed a 36% increase in brain/body weight ratio, thus exhibiting macrocephaly. Closer examination revealed the presence of giant neurons in the cortex that resembled the cortical tubers frequently observed in human TSC patients (Figure 3.12A). In addition, the dentate gyrus in *Tsc1* mutants was obviously enlarged. Further analysis indicated increased thickness of mossy fiber tract and molecular layers, suggesting axonal and dendritic hypertrophy (Figure 3.12 B-C). Also P-S6 levels were increased in the cortex and hippocampus of *Tsc1* mutant mice, reflecting robust activation of mTOR signaling (Figure 3.12D). All of these changes are similar to those observed in *Pten* mutant mice. These independent genetic data further support the key role of the PI3K/AKT/mTOR pathway in mediating the anatomical defects seen in our mutant mice.

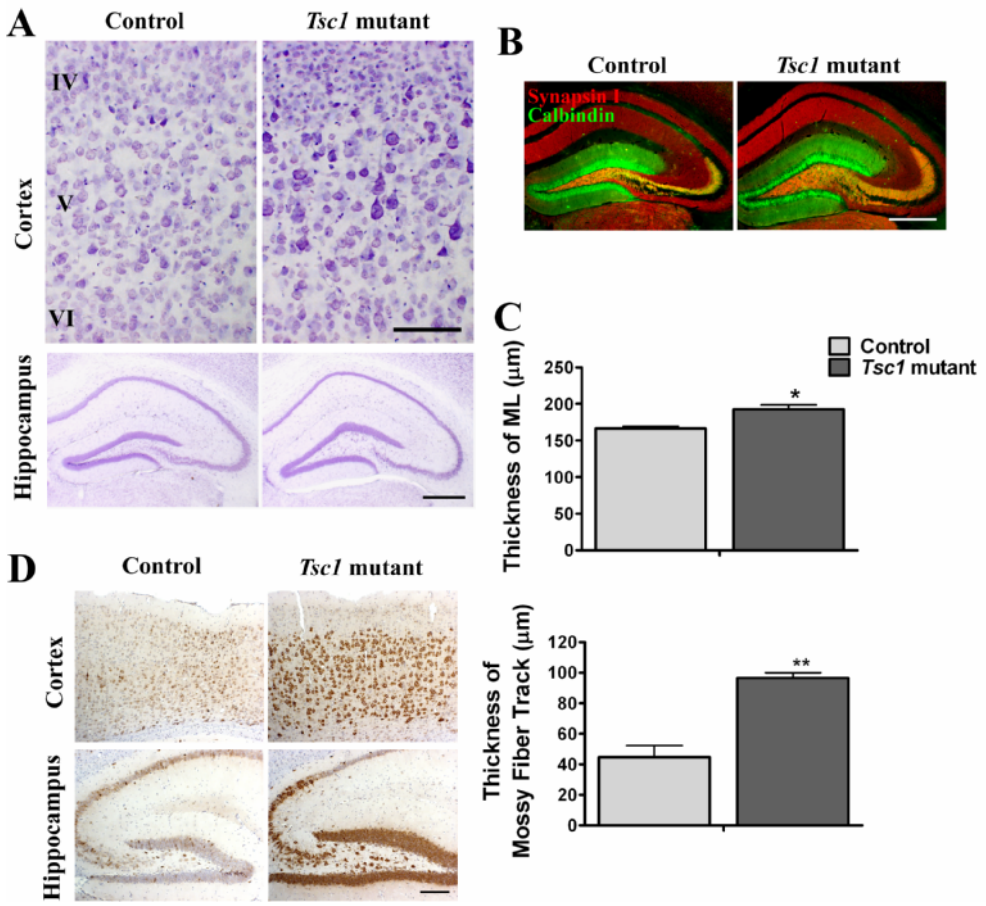

Figure 3.12 loss of *Tsc1* causes similar neuronal hypertrophy phenotype as *Pten* loss. (A) Nissl staining reveals cortical tubers and enlarged hippocampal structure in *Tsc1* mutant mice. Scale bar, 100μm and 500μm respectively. (B) Immunostaining shows increased thickness of mossy fiber tract in *Tsc1* mutant mice. Scale bar, 500 μm. (C) Quantification reveals increased thickness of mossy fiber tract and molecular layer in *Tsc1* mutant mice. n=3 mice per group. Data are

mean ± SEM and analyzed by *t*-test. *p<0.05 and **p<0.01, as compared to control. (D) *Tsc1* mutant mice have increased P-S6 signal in the cortex and hippocampus. Scale bar, 200 μm.

Discussion

The development and use of murine models for the purpose of replicating and better understanding human disease has gained considerable ascendance in recent years. Here, we take advantage of murine models to attempt to better understand the etiology of human macrocephaly and autism when associated with the PI3K/AKT signaling pathway.

The PI3K/AKT/mTOR pathway and neuronal morphology

The abnormal behaviors observed in *Pten* mutant mice are accompanied by overgrowth of the cortex and hippocampus and changes in neuronal morphology, including hypertrophy and loss of polarity. In the current study, we tried to further dissect PI3K/AKT downstream signaling with particular focus on the TSC/mTOR pathway.

First, we found that blocking the TSC/mTOR downstream pathway in *Pten* mutants dramatically reversed the soma, dendritic and axonal hypertrophy. Second, in *Nse-cre*; *Tsc1* $^{loxP/loxP}$ *mice*, we observed similar cellular hypertrophy. Unfortunately, our *Nse-cre;Tsc1*$^{loxP/loxP}$ mice failed to thrive and the majority died before adulthood, precluding further behavioral tests. We believe death results from kidney failure, although this has yet to be rigorously ascertained (data not shown). Nonetheless, the few *Nse-cre;Tsc1*$^{loxP/loxP}$ mice that survived into

adulthood exhibited anatomical and cellular abnormalities that closely paralleled that of the *Pten* mutant mice. Taken together, these studies underscore the importance of the PI3K/AKT/mTOR pathway in controlling the neuronal hypertrophy described in this study.

When applied to presymptomatic *Pten* mutants, rapamycin suppressed the appearance of Synapsin I staining in the molecular layer, a sign of loss of polarity of granule cells. However, in older mice, rapamycin did not reverse this effect, as shown by both Synapsin I and Golgi staining. Interestingly, we do not observe ectopic Synapsin I staining in *Tsc1* conditional knockout mice, although mTOR signaling is highly activated. These data suggest that PI3K/AKT downstream pathways other than TSC/mTOR may be responsible for maintaining neuronal polarity. GSK3β, a direct AKT target, is an attractive candidate since it is activated in the *Pten* mutants and is known to play important roles in the establishment and maintenance of neuronal polarity *in vitro* (Jiang et al., 2005). It is worth noting that *in vivo* there may exist functional redundancy with other GSK3s, since knocking out *Gsk3β* does not to cause apparent neuronal defects (Kim et al., 2006).

Beneficial effects of rapamycin on behavior

We previously reported that *Pten* mutant mice exhibit a variety of abnormal behaviors including anxiety, social interaction deficits, and sporadic seizures (Kwon et al., 2006a; Ogawa et al., 2007). The dramatic activity of rapamycin in reversing cellular abnormalities motivated us to examine whether treatment would also have a beneficial effect on behavior. However, restricted by the limited time window, we could only perform a few behavioral tests instead of an extensive examination. In addition, we suspected that chronic daily injection of rapamycin might alter behavior directly as a consequence of stress placed on the mice. This effect might well be amplified in the mutant mice that already exhibit increased anxiety. We found the older mutant mice were more vulnerable to handling and increased mortality during the period of injection was frequently observed, making the tests very difficult to perform. However, it was reassuring that rapamycin treatment did have a measurable beneficial effect on the behavior of the young cohort. This effect was particularly striking in the social interaction task, in which rapamycin paradoxically enhanced social interaction in mutants while decreasing social interaction in wild-type controls.

The EEG recording for seizure activity is the most objective measurement and relevant to disease, since 20-25% of autism patients have seizures which can be life-threatening (Canitano, 2007). We were surprised by the degree to which rapamycin administration was able to reverse both the seizure frequency and

duration. The anti-seizure effect of the drug was observed as early as the first week of treatment and remained throughout the 4-week drug administration period. In contrast, *Pten* mutants treated with vehicle demonstrated higher seizure frequency and duration, with two of six mice perishing during the injection period. These data reveal that rapamycin is a potentially useful seizure treatment modality for autism patients, particularly for those bearing germline *PTEN* or *TSC1/2* mutations. We were gratified to see that as our manuscript was in preparation, a study from Kwiatkowski's group further demonstrated that applying rapamycin in *Synapsin I-cre; Tsc1*$^{loxp/loxp}$ mice could successfully control seizures and prolong the survival of mutant mice, further supporting our findings here (Meikle et al., 2008).

Feedback effects of rapamycin in the context of Pten loss

Recently, long-term rapamycin treatment has been shown to be capable of inducing inhibitory feedback effects on AKT activity through exclusion of the mTOR molecule from the TORC2. We showed that AKT activity is attenuated in the cortex and hippocampus after chronic rapamycin exposure (Figure 3.11A&B). Thus, rapamycin affects not only mTOR but also may decrease AKT activity. Other strategies will have to be employed to assess the relative contribution of non-mTOR effectors to the phenotypes studied here.

Concluding remarks

The relationship between abnormal rodent behaviors and human neuropsychiatric disorders is tenuous. Nonetheless, by targeting mutations known to cause human brain dysfunction to specific anatomic areas, and then analyzing the resulting morphological and behavioral abnormalities, we may glean important information about the anatomical and cellular underpinnings of relevant disorders. In the present context, we have achieved such a link. Further, we have provided evidence for a potential therapeutic window in certain cases of ASD.

Chapter IV: TSC1 mediates polycystic kidney disease

Background:

As mentioned in general introduction, increasing evidence suggests the involvement of the TSC/mTOR signaling in the development of PKD. However, some questions are still waiting to be addressed. How exactly is the dysregulation of the TSC/mTOR pathway involved in PKD? What is the relationship between the TSC/mTOR pathway and polycystin proteins? Does the TSC/mTOR pathway work downstream, upstream or parallel of polycystin proteins? The interesting findings from Eker rats (with *Tsc2* deletion) suggested that loss of *Tsc2* could disrupt the membrane localization of Polycystin-1 protein. Thus, the cellular function of Polycytine-1 could be TSC2 dependent. However, it could not explain the increased mTOR activity observed in *Pkd1* conditional knockout mice and PKD patients, and further the inhibitory effect of rapamycin on the cyst formation in *Pkd1* conditional knockout mice (Shillingford et al., 2006). Furthermore, only a small percentage of Eker rats develop PKD depending on spontaneous loss of heterozygosity of *Tsc2* during early embryogenesis (Cai et al., 2003). Therefore, the Eker rat is not a stable PKD animal model, which makes further *in vivo* study difficult.

We feel that the first step for addressing above questions is to establish a stable PKD model by directly targeting components of the TSC/mTOR pathway,

which will not only confirm the involvement of the TSC/mTOR pathway in PKD, but also provide a chance to understand how it is involved by examining abnormalities of renal cells during the process of cystogenesis. Furthermore, we know TSC1 and TSC2 function as a complex, but so far there is no evidence suggesting the involvement of TSC1 in PKD. *TSC2* and *PKD1* are linked on the same chromosome both in human and mouse with only 60bp in between. Therefore, accidentally disrupting the *Pkd1* gene is always a concern when genetically manipulating the *Tsc2* gene. Thus, to generate a mouse model to study the function of the TSC/mTOR pathway in PKD, the *Tsc1* gene might be a better target.

Here, we generated a PKD mouse model by knocking out *Tsc1* only in a subset of renal tubule cells. Further characterization of the *Tsc1* conditional knockout mice revealed mTOR overactivation in the cyst-lining cells accompanied by abnormal cellular morphology occurring at the very beginning of cytogenesis. More importantly, we found inhibition of mTOR with low dosage of rapamycin administration could effectively block the cyst formation. Finally, we showed that in a same context, knocking out *Pten*, an upstream negative regulator of mTOR, could not result in polycystic kidneys due to limited activation of mTOR, suggesting distinct effects on mTOR activation for PTEN and TSC1 in renal tubule cells.

Results:

Tsc1 mutant mice have increased mortality due to development of severe polycystic kidney disease:

We previously developed a *Nse-cre* mouse line that bears cre activity mainly in subsets of post-mitotic neurons in the brain, as well as in limited cells in the kidney and testis (Kwon et al., 2006b). We generated the *Tsc1* conditional knockout mice (*Tsc1* mutant mice hereafter) by crossing $Tsc1^{flox}$ mice (Meikle et al., 2007) with the *Nse-cre* line, initially aiming to further assess the function of the TSC/mTOR pathway in the nervous system. Surprisingly, the resulting *Tsc1* mutant mice, though appeared normal at birth, soon became distinguishable from their littermates by notable smaller body size and distent abdomen (Figure 4.1A). This surprised us, as in the brain the *Nse-cre* activity is mainly developed postnatally and is not fully activated until 4 weeks of age, whereas *Tsc1* mutant mice were apparently smaller by 3 weeks of age compared to littermate controls (Figure 4.1B). In addition, mutant mice had increased mortality starting from 3-4 weeks of age (Figure 4.1C). Further examination revealed that *Tsc1* mutant mice developed severe polycystic kidneys (Figure 4.1D). Despite the fact that there were variations among individuals in terms of the extent of cyst development, the phenotype had full penetrance and always appeared bilaterally. Furthermore, we found that cysts were formed mainly in the cortex, while the collecting ducts are largely intact. This massive cyst formation in kidneys accompanied by increased

blood urea nitrogen (BUN) level, suggesting that the reduced viability in mutants was due to renal failure (Figure 4.1E).

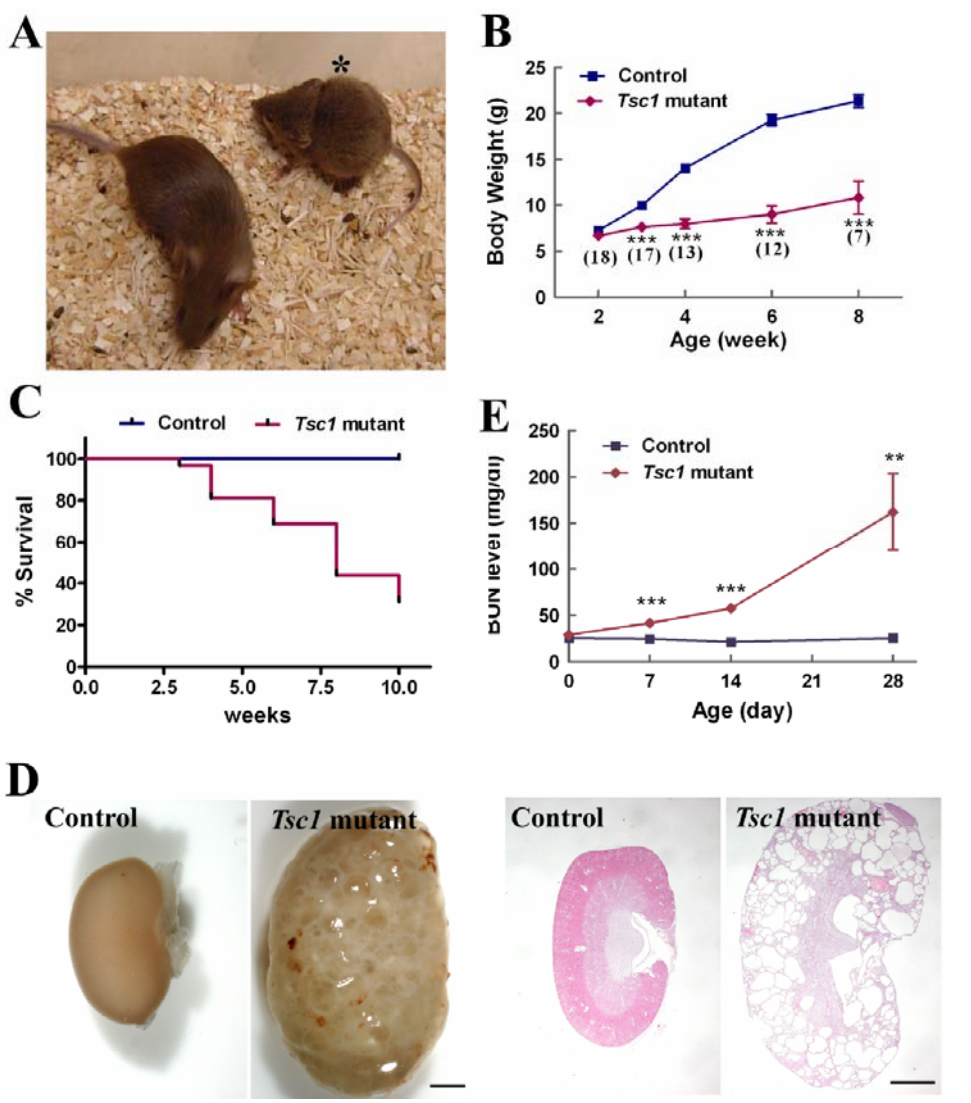

Figure 4.1 *Tsc1* mutant mice show reduced viability due to development of polycystic kidneys. (A) Representative picture of *Tsc1* mutant mouse (asterisk) and littermate control at P28. Mutant mice display smaller body size and distent belly. Scale bar, 2 mm. (B) *Tsc1* mutant mice show growth retardation after 2

weeks of age. n=15 controls, n=18 *Tsc1* mutants at the beginning. (C) Survival curve shows reduced viability of *Tsc1* mutant mice. n=27 controls, n=32 *Tsc1* mutant. (D) Gross appearance and H&E staining of the polycystic kidney developed in *Tsc1* mutant at P28. (E) Reduced viability was accompanied by progressive renal failure in *Tsc1* mutants, as shown by dramatically increased BUN level along postnatal development. n=7 animals per group were examined at each time point. Graphs are plotted by mean± SEM. Data is analyzed by Student *t*-test. *p<0.05, **P<0.01 and ***P<0.001, as compared to littermate control.

Nse-cre activity is induced along the nephrogenesis

Previously, we reported the *Nse-cre* expression pattern and noticed cre activity in the kidney (Kwon et al., 2006b). However, the characterization was mainly focused on the nervous system. Driven by the interesting finding in *Tsc1* mutant mice, we felt it necessary to have a detailed examination of *cre* expression in the kidney. In consistent with previous report, we found that cre activity in the kidney was largely restricted in the cortex in a fully developed kidney as shown by using *Rosa-stop-lacZ* reporter mice (Soriano, 1999) (Figure 4.2A). We further examined the morphology of cre^+ cells under higher magnification view of X-gal staining. Interestingly, cre^+ cells were found mainly in the renal tubule cells and only a few in the renal corpuscles (Figure 4.2A right panel).

By examining *cre* expression during early embryonic stages, we found cre activity was induced along nephrogenesis (Figure 4.2B). It could be detected as early as E11.5 in the mesenchymal blastema that surrounds the ureteric bud (asterisk). However, the signal was very weak. *cre* expression usually became evident at E12.5, observed exclusively in the outer layer of the metanephric kidney, where nephrogenesis occurs. Cre^+ cells were mainly restricted in the dense cell clusters surrounding ureteric buds (asterisk) and also seen in some newly induced nephrons (arrowhead). In the following several days, cre expression was continuously induced in nephrogenic zone, observed frequently in

the coma and S-shaped bodies that would become nephrons. The induction of *cre* expression continues during the first few days after birth. However, we did observe variation among individuals in terms of the percentage of cells bearing cre activity. At P7, roughly 5-10% of total renal cells were cre^{+}, as evaluated by FACS analysis using *Rosa-stop-yfp* reporter mouse line (Figure 4.2C).

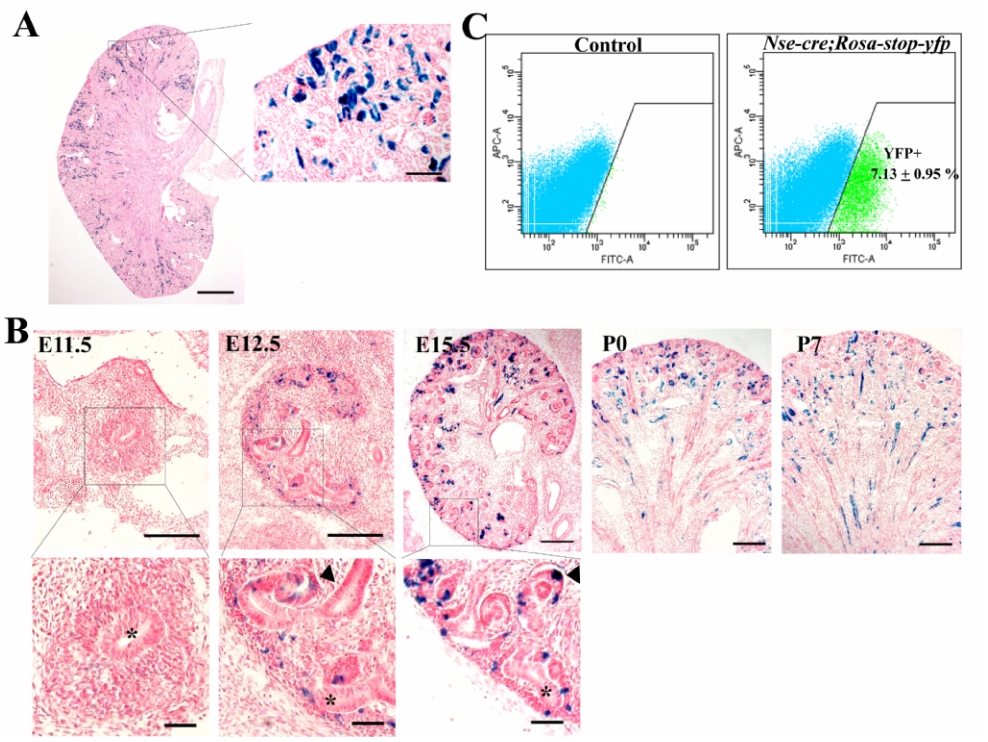

Figure 4.2 *Nse-cre* expression in the kidney. (A) The *Nse-cre* expression pattern in the kidney is demonstrated by X-gal staining of a kidney of *Nse-cre; Rosa26-stop-lacZ* mouse at P28. Left panel shows high magnification view of the boxed area. Scale bar, 1 mm or 100 μm respectively. (B) *cre* expression is developed along nephron induction in the early embryonic stages. Ureteric bud (asterisk); newly induced nephrons (arrowheads). Scale bar, 200 μm for upper panels and 50 μm for lower panels. (C) Only a subset of renal cells bear cre activity as shown by FACS sorting analysis using *Nse-cre; Rosa-stop-yfp* mice at P7. n=4 mice were used per group.

Tsc1 mutant mice develop severe polycystic kidneys progressively after birth

To get a clear view of cyst development, we examined kidneys in *Tsc1* mutant mice at the different time points. To our surprise, we found that at P0 mutant kidneys were anatomically normal, though slightly enlarged in size (Figure 4.3A). This suggested that loss of *Tsc1* in a subset of renal tubule cells did not affect overall kidney development. However, mutant mice developed polycystic kidneys progressively during the first few weeks after birth (Figure 4.3B). Although the onset of cyst formation might vary in different individuals, cysts were usually observed by P7. The initial cyst formation was commonly seen in the inner cortex, and cysts were found surrounded by pink color tubule cells in H&E staining, indicating the proximal tubule origin of these initial cysts. Cysts developed quickly in the following week with increases both in number and size. At P14, cyst formation was widely observed in the cortex, but still restricted to renal tubules leaving glomeruli largely intact. At P28, most cysts were further dilated and surrounded by a very thin layer of epithelial cells. In addition, increased interstitial fibrosis was observed along cyst formation, which appeared as early as P7 and filled almost all the inter cysts space in the later stages (Figure 4.3B, low panels). Massive cyst formation resulted in substantial increase of renal volume as reflected by dramatically increased kidney weight (Figure 4.3C).

Interestingly, we also frequently observed cysts filled with multiple layers of epithelial cells (Figure 4.4). In some dramatic cases, cysts were full of cells, forming a tumor like structure. Under higher magnification view, it was easy to define mitotic figures in the tumor-like mass. Multiple layers of epithelial cells were also seen to accumulate in the corner of some cysts. Among those cells, we occasionally observed a huge vacuole inside a cell that pushed the nucleus to the edge. These resemble features of human renal cell carcinoma.

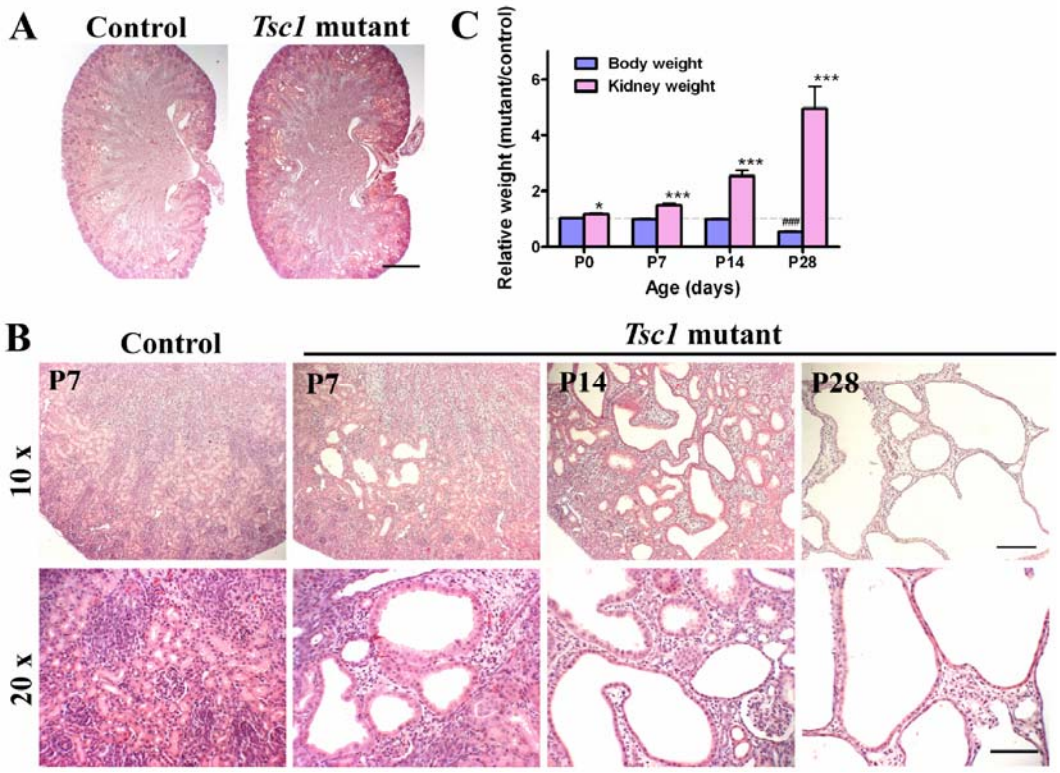

Figure 4.3 *Tsc1* mutant mice develop PKD progressively after birth. (A) At P0, kidneys of *Tsc1* mutant mice have normal structure but enlarged in size. Scale bar, 500 μm. (B) H&E staining shows that *Tsc1* mutant mice develop PKD progressively after birth. Scale bar, 200 μm for upper panels and 100 μm for lower panels. (C) Development of PKD in *Tsc1* mutant results in dramatically increased kidney weight, compared to controls. n=15 pairs for P0, and n=10 pairs for the other time point. Data are plotted by mean± SEM and analyzed by Student *t*-test. *p<0.05, **P<0.01 and ***P<0.001, as compared to littermate control.

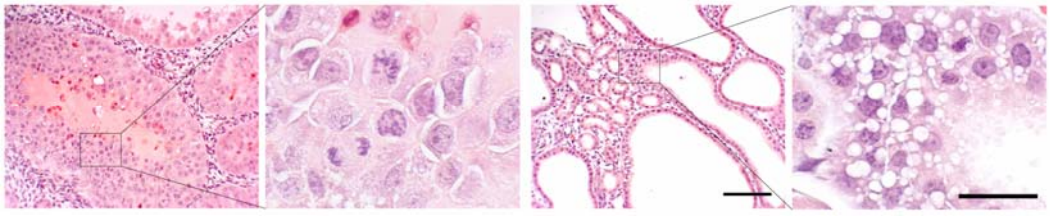

Figure 4.4 *Tsc1* mutant mice develop cysts accompanied by features of renal cell carcinoma as shown by detailed examination at P14. Scale bar, 100 μm for lower magnification view and 25 μm for higher magnification view of boxed area, respectively.

cre positive cells get expanded in the kidneys of Tsc1 mutants

Among all these interesting abnormalities, we were particularly interested in the cyst formation, as it was the most dramatic phenotype and likely the main cause of renal failure. However, we were surprised by the broad cyst formation, since we were only targeting a small percentage of renal tubule cells. Due to lack of reliable anti-TSC1 antibody for immunostaining, we again took the advantage of reporter lines for monitoring cre-mediated recombination both in controls and *Tsc1* mutants. Interestingly, at P7, we observed obvious increased Yfp^+ cells in the kidney of *Tsc1* mutants compared to that in littermate controls when using *Rosa-stop-yfp* reporter line (Figure 4.5 A). This observation was quantified by FACS analysis (Figure 4.5B). The percentage of Yfp^+ cells increased about three folds in *Tsc1* mutants with 15-30% of total renal cells in contrast to only 5-10 % in controls. We examined the proliferation of Yfp^+ cells at P7. Interestingly, there are no obviously increased Yfp/BrdU co-labeling cells in mutants, compared to controls (data not shown). On the other hand, we did not detect apparent apoptosis before P7 both in controls and mutants (Figure 4.6). We suspected that in the mutants, *Tsc1*-null cells somehow expanded in population before renal tubule cells fully differentiated. However, this needs to be further confirmed.

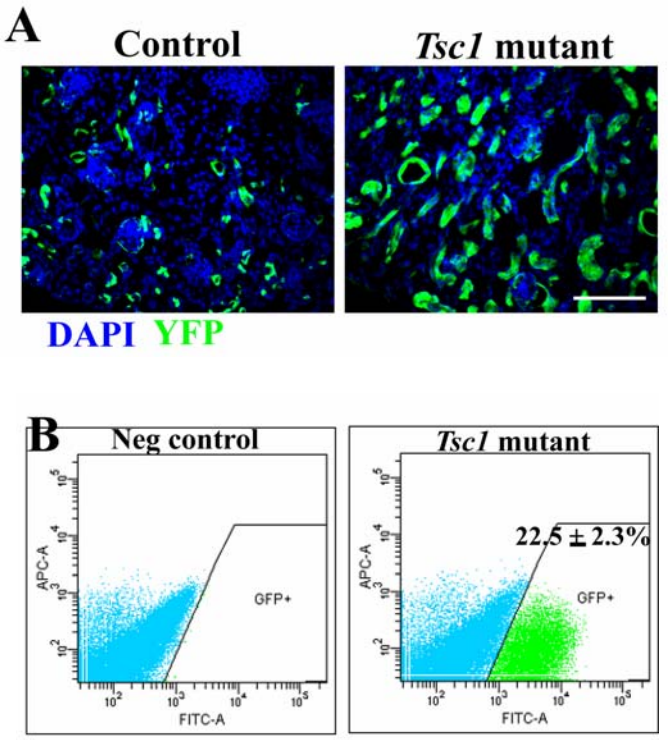

Figure 4.5 *Tsc1* loss results in self-expansion. (A) Renal tubule cells that lose *Tsc1* expended in population, as visualized by Yfp immunostaining both on control and *Tsc1* mutant mice bearing a *Rosa-stop-yfp* allele at P7. Scale bar, 200 μm. (B) An increased percentage of Yfp^+ cells in *Tsc1* mutants is confirmed by FACS sorting analysis. n=4 mice at P7 were used per group.

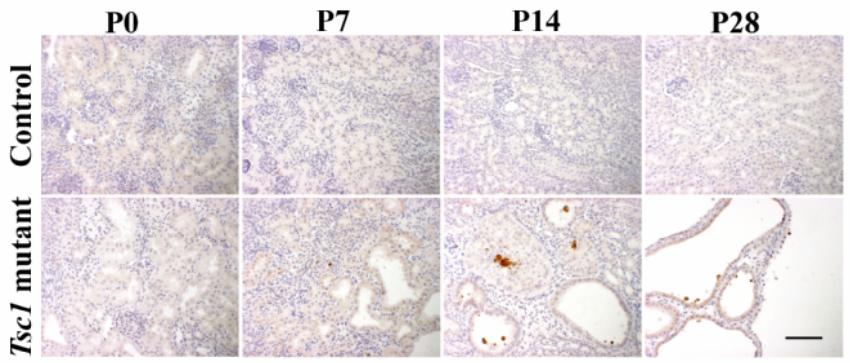

Figure 4.6 Increased apoptosis is observed along cyst formation. Cleaved Caspase-3 staining appears increased in *Tsc1* mutants after P14. Cells under apoptosis are the renal epithelial cells. Scale bar, 100μm.

Loss of Tsc1 results in overactivation of mTOR

We know that the primary consequence of *Tsc1* loss is increase of mTOR activity. So, we assessed the activity of mTOR complex, which was evaluated by two mTOR downstream effectors, P-S6 and P-4E-BP1. We first performed Western blotting by using cell lysate from whole kidneys of either controls or mutants. As shown in figure 4.7 A, increased P-S6 and P-4EBP1 levels in the mutants were already obvious at P0 and became more dramatic at P7. However, the activity of the PI3K/AKT pathway, one of the upstream pathways of TSC, was not affected as reflected by unchanged P-AKT level between control and mutant samples. At the same time, we did observe increased total protein levels in mutants for some proteins, such as apparent elevated total 4EBP1 level and trend of increase in total AKT level. We suspected that it might be due to the interference with general protein translation machinery after *Tsc1* loss. On the other hand, the crosstalk with other translation machinery might result in differences among each distinct protein. Still, this needs to be further evaluated in our system. Nevertheless, to make a reasonable comparison, the amount of protein loaded for each sample was carefully controlled and both α-tubulin and β-actin were used as loading controls. The increased P-S6 level was further confirmed by immunostaining (figure 4.7B). Interestingly, loss of *Tsc1* caused overall increase of P-S6 level in the cortex. Although we noticed that there was certain basal level of P-S6 signal in the controls at P7, we observed stronger and broader P-S6

staining patterns in the mutants. At P14, P-S6 signal in control groups was reduced with only minimal staining in the cortex, while in the mutants P-S6 staining was further increased with almost all of the cyst-lining cells showing P-S6 staining.

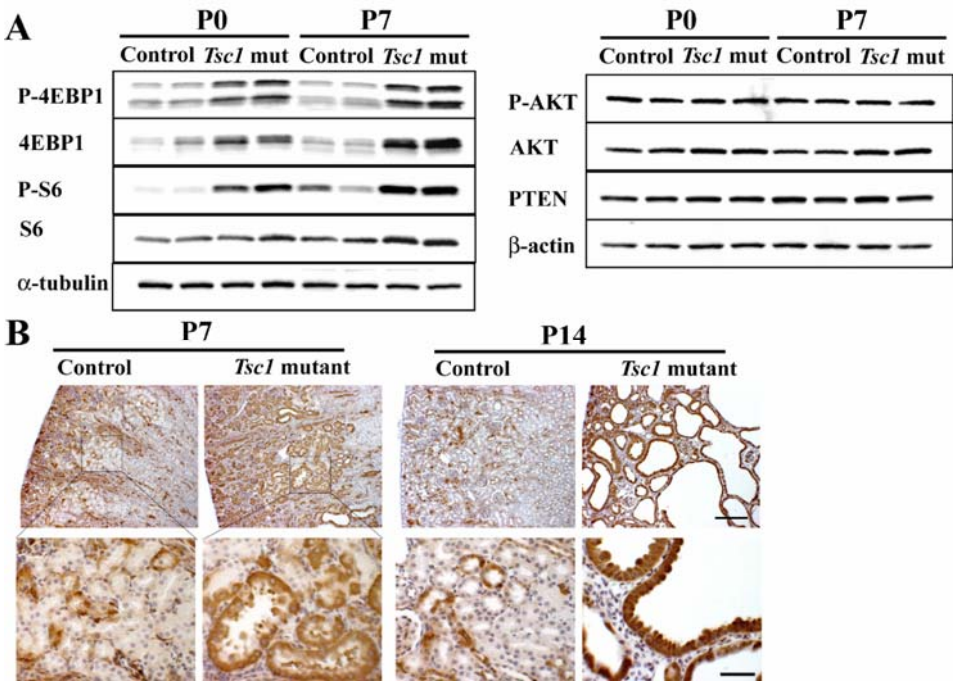

Figure 4.7 loss of *Tsc1* in a subset of renal tubule cells results in a broad increase of mTOR signaling. (A) Western blotting analysis reveals dramatic activation of mTOR signaling in *Tsc1* mutant mice. n=3 pairs were examined at each time point. (B) P-S6 immunostaining on P7 and P14 kidneys from the control and *Tsc1* mutant mice. Scale bar, 200 μm and 50 μm respectively.

Cyst-lining cells with elevated P-S6 staining demonstrate abnormal morphology

We further focused on the cyst-lining cells, since it has been proposed that abnormalities of those cells are associated with the cyst formation in other PKD models. Not surprisingly, cyst-lining cells that lose *Tsc1* demonstrated dramatically elevated P-S6 signaling, as shown by increased coincidence of Yfp and P-S6 labeling in mutants, compared to that in controls (Figure 4.8 A). In the mutants, we observed that all Yfp+ cyst-lining cells were co-labeled with strong P-S6 staining. However, surprisingly, we also found out that not all cyst-lining cells were Yfp positive, although they were P-S6 positive (Figure 4.8A, arrowheads). This argued that the cyst formation was not only restricted to the tubule cells that lose *Tsc1*, indicating the involvement of non-cell autonomous effects for mTOR activation.

Down regulation of TSC1/TSC2 or increased mTOR activity results in increased cell proliferation and cellular hypertrophy in different cell types (Wullschleger et al., 2006). We further assessed the effects of *Tsc1* loss on the proliferation and morphology of the cyst-lining cells. As renal tubule cells in different nephron segments are structurally different, we used the proximal tubule as an example. We particularly focused on the inner cortex, where cysts were initially observed. Interestingly, some proximal tubules in *Tsc1* mutants were more swollen than those in the controls (Figure 4.8B). Frequently, we observed

swollen tubule cells bear huge nuclei (arrow, Figure 4.8B). The enlarged cell size was not due to cell mitosis arrest, since those cells were negative for BrdU staining. On the other hand, we did not observe dramatically increased proliferation in cyst-lining cells.

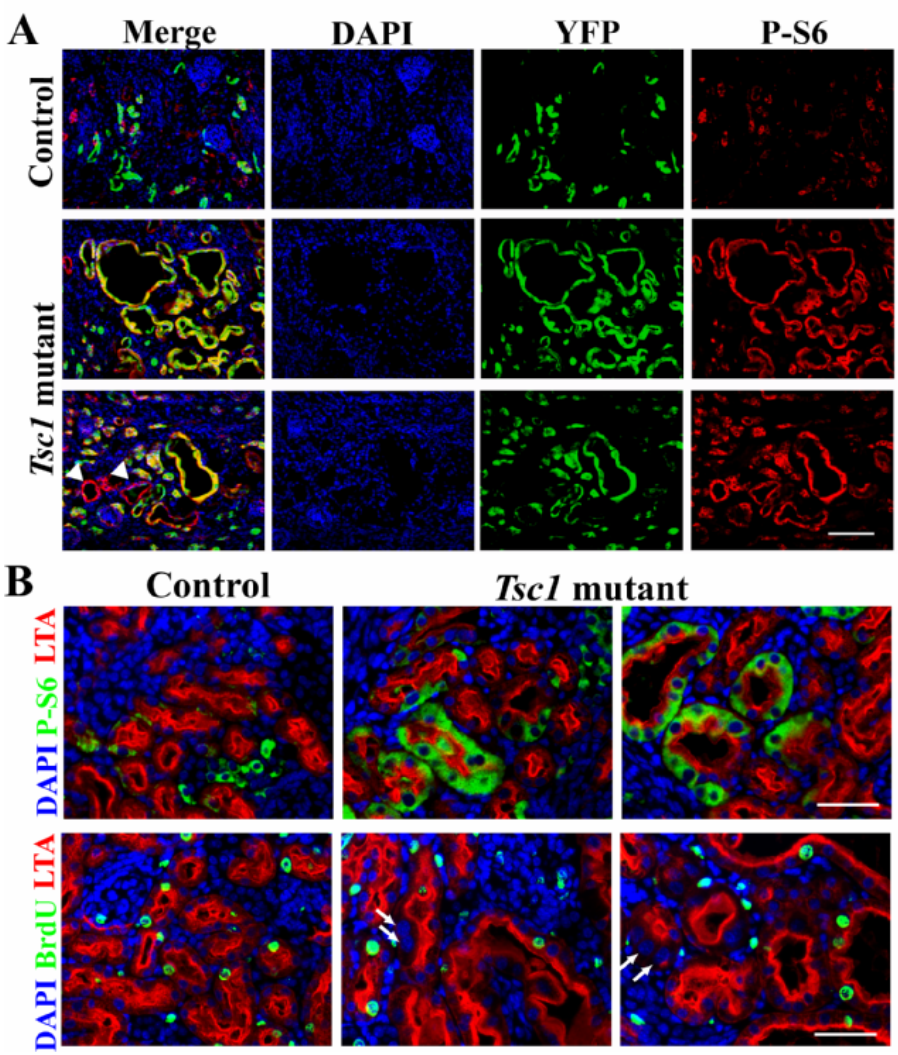

Figure 4.8 The cyst-lining cells with increased P-S6 staining demonstrate abnormal morphology. (A) P-S6 (red) and Yfp (green) immunostaining on P7 kidneys from controls and *Tsc1* mutants, suggesting elevated P-S6 staining in the cyst-lining cells. Scale bar, 100 μm. (B) Increased P-S6 staining (green) are correlated with abnormal morphology of the cyst-lining cells, as demonstrated using the proximal tubule (LTA stained, red). Scale bar, 50 μm.

Rapamycin treatment inhibits the cyst formation

If the abnormal activation of mTOR was responsible for the cyst formation, we would be able to block the cyst formation by applying mTOR specific inhibitor, rapamycin. Rapamycin administration for blocking mTOR activity has been widely used in humans and mice. However, we found that applying high dosages of rapamycin during the early postnatal stages had severe adverse effect with mice showing obvious growth retardation (data not show). We finally used 2 mg/kg rapamycin. Mice were injected with rapamycin at P8 and collected at P14. Surprisingly, we found that cyst formation was inhibited dramatically by single rapamycin administration. Kidneys of rapamycin-treated mutants demonstrated either limited cysts formation (2 out of 6 mutants) or no cysts (4 out of 6 mutants), in contrast to the broad cyst formation in mutants treated with vehicle (Figure 4.9A). In addition, rapamycin treatment normalized the kidney weight with only a slight effect on the body weight (Figure 4.9B). Therefore, the cyst formation is largely relied on mTOR activity. However, this inhibition was drug dependent. Without further rapamycin administration, mutants would develop PKD eventually (data not shown).

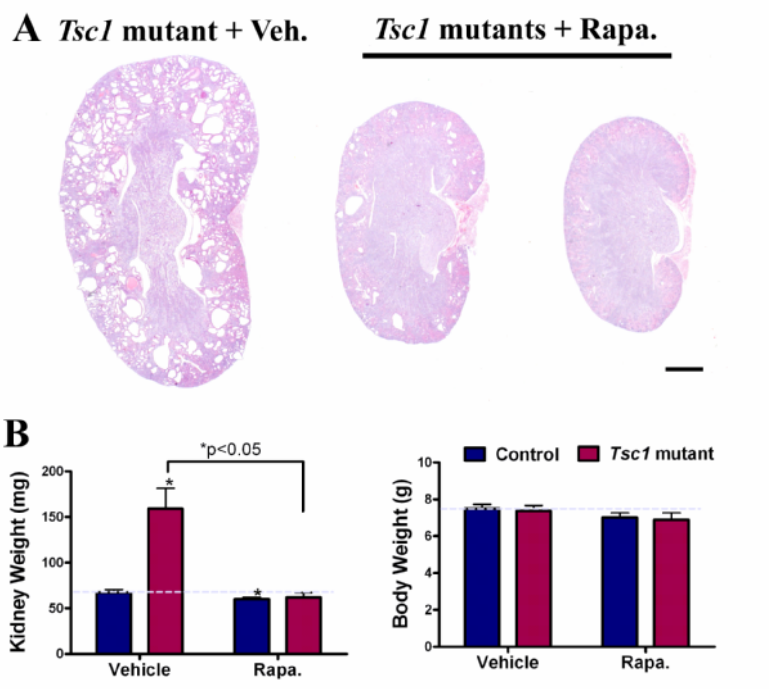

Figure 4.9 Rapamycin treatment inhibits the cyst formation and controls the cyst development. (A-B) Control and *Tsc1* mutant mice were treated with either vehicle or 2 mg/kg rapamycin at P8 and examined at P14. (A) H&E staining reveals that rapamycin effectively inhibits the cyst formation in *Tsc1* mutants. N=6 mice per group (B) rapamycin injection normalized the kidney weight of *Tsc1* mutants, while slightly reduced the body weight. N=6 Data are plotted by mean± SEM and analyzed by Student *t*-test. *p<0.05, as compared to littermate control.

Loss of Pten in a similar context does not develop PKD

Previously, we used the same *Nse-cre* line to study the function of PTEN in neurons (Kwon et al., 2006a). It has been well established that *Pten* loss results in overactivation of AKT, which in turn inhibits TSC complex and activates mTOR. Surprisingly, we did not notice apparent renal abnormalities in *Pten* mutant mice in our previous study. To confirm previous observation, we did more careful characterization on the kidneys of *Pten* mutants and reached the same conclusion. The kidneys from *Pten* mutants appeared normal as shown by H&E staining (Figure 4.10A), although they did show a slight increase in size along the growth of mice, as quantified by a small increase in the kidney weight by P28 (Figure 4.10B). There was no cyst formation among all four mutants sectioned at P28, which consisted with the normal BUN levels observed in a larger group of mutant mice (Figure 4.10C).

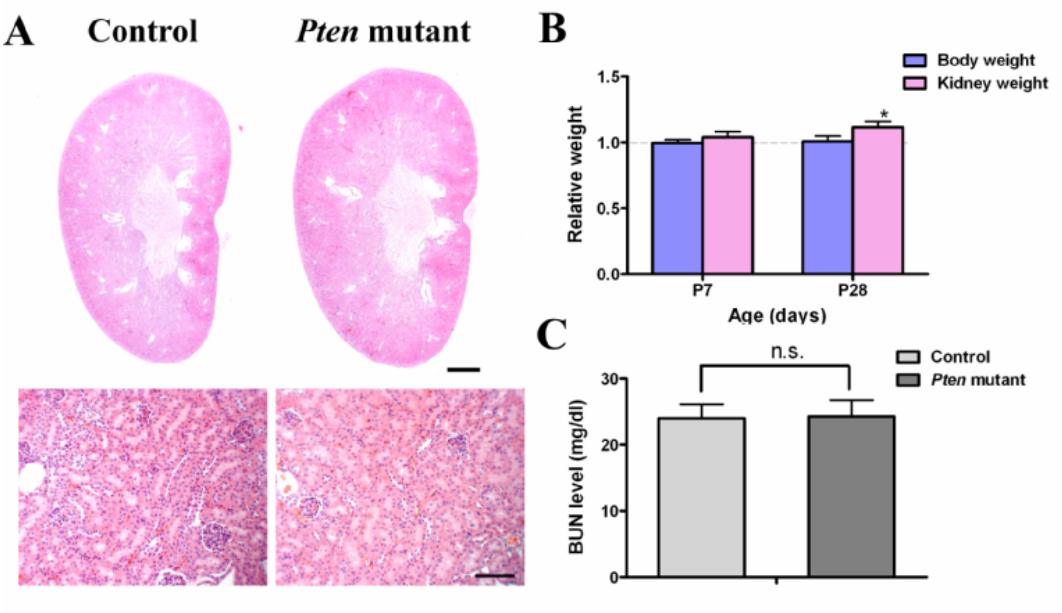

Figure 4.10 *Pten* mutant mice do not develop PKD. (A) *Pten* mutant mice develop normal kidney structure with no sign of PKD. Upper panels are representative H&E staining pictures indicating normal kidney structures in *Pten* mutant mice at P28. Lower panels show the normal organization of the renal tubule cells in *Pten* mutants under higher magnification view. Scale bar, 1 mm for upper panels and 100 μm for lower panels. (B) *Pten* mutant mice develop normal body weight, but slightly hypertrophic kidney by 4 weeks of age. n=6 for each group. (C) *Pten* mutant mice have normal renal function as suggested by the normal BUN levels. n=7 mice for each genotype. Data are mean ± SEM and analyzed by paired *t*-tests. *$p<0.05$, as compared to controls and n.s. stands for not significant.

There are several possibilities that might explain what happened. First, we thought this could be due to different genetic background of mouse strains. Secondly, TSC complex is only one of the AKT downstream pathways. It is possible that the other AKT downstream pathways compromised mTOR activity and inhibited the cyst formation. However, these two possibilities were excluded by the fact that double mutants (*Nse-cre;Pten*$^{loxP/loxP}$*;Tsc1*$^{loxP/loxP}$) developed PKD as well as *Tsc1* mutants, which led to postnatal lethality even more severely than loss of *Tsc1* alone. On the other hand, in the same breeding, *Nse-cre;Pten*$^{loxP/loxP}$*;Tsc1*$^{loxP/+}$ mice did not have renal problem with no sign of increased mortality (Figure 4.11A). This leaves to one obvious question, that is, whether mTOR is equally activated in *Pten* and *Tsc1* mutants. Particularly, we know that TSC complex is regulated by multiple upstream pathways besides the PI3K/AKT pathway (Tee and Blenis, 2005; Wullschleger et al., 2006). Interestingly, we found that loss of *Pten* in a similar context did not effectively cause mTOR activation as *Tsc1* loss, which was first demonstrated by Western blotting (data not shown). There is no clear trend of increase on P-AKT and P-S6 levels in *Pten* mutants during the early postnatal stages, although there were variations among samples. This could be partially explained by the fact that *Pten*-null cells did not get dramatic self-expansion in the first place. When using *Rosa-stop-yfp* reporter line, only ~10% of total renal cells were Yfp+ in *Pten* mutant kidneys, which was slightly higher than that in controls, but significantly less than

that in *Tsc1* mutants (Figure 4.11B). We suspected that the increased P-AKT and P-S6 levels in a subset of renal tubule cells could be averaged out when using whole kidney lysate for Western blotting. Therefore, we performed immunostaining for P-S6. Surprisingly, we did not see obvious elevated P-S6 signal when comparing controls and *Pten* mutants at P7, although clearly increased P-S6 staining in *Pten* mutants was detected at P28 (Figure 4.11C). It is likely that loss of *Pten* dose not develop PKD due to limited activation of mTOR during early development.

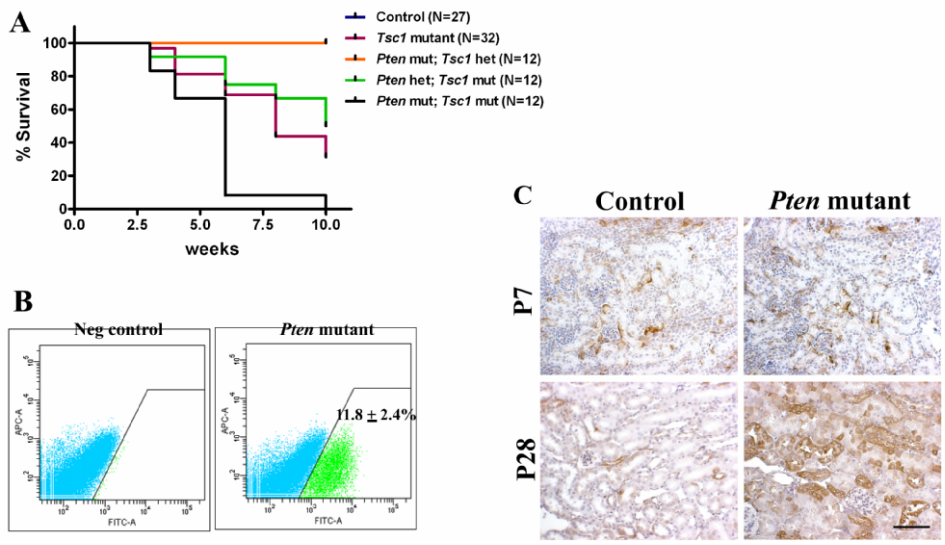

Figure 4.11 Loss of *Pten* in the renal tubule cells results in limited activation of mTOR during the early postnatal stages. (A) Survival curve of *Pten* and *Tsc1* double mutant mice. (B) Renal cells that lose *Pten* get slightly increase in population, as visualized by FACS analysis of Yfp+ cells in *Pten* mutant mice bearing a *Rosa-stop-yfp* allele at P7. n=3 (C) Loss of *Pten* in the renal tubule cells results in limited activation of mTOR during early postnatal stage, as shown by immunostaining of P-S6. Scale bar, 100 μm.

Discussion:

Tsc1 mediates polycystic kidney disease

In the current study, we generated a mouse PKD model by conditionally knocking out the *Tsc1* gene in a subset of renal tubule cells. This, together with previous observations in some of Eker rats (Kleymenova et al., 2001), strongly suggests the involvement of TSC1/2 complex in the development of PKD. In addition, by carefully examining our *Tsc1* mutants, we found that massive cyst formation was accompanied by dramatically increased mTOR activity in the cyst-lining cells due to both cell autonomous and non-cell autonomous effects. Increased mTOR activity results in abnormal morphological changes of renal tubule cells in the early stages of cystogenesis. Furthermore, inhibition of mTOR activity by rapamycin effectively suppresses the cystogenesis and cyst development. Therefore, mTOR overactivation is important for both initiating and maintaining renal cysts.

On the other hand, in our study, loss of *Tsc1* by cre-mediated recombination starts in early embryonic stages, which results in the early onset of cyst formation, fast cyst development and further increased mortality in early postnatal stages. This phenotype resembles the severe infantile PKD cases in humans due to continuous TSC2 and PKD1 gene deletion, suggesting the involvement of mTOR signaling in this continuous deletion syndrome. Thus, our study might shed light on the possible treatment of this syndrome.

Distinct roles of PTEN and TSC1 in renal tubule cells

In chapter III, we described how PTEN and TSC1 work in concert to control neuronal hypertrophy. Here, we report their distinct roles in renal tubule cells. Unlike *Tsc1* mutants, *Pten* mutants do not develop PKD in the same context. Further study suggests that this might be due to the limited activation of mTOR signaling after *Pten* loss in the early postnatal kidney. Thus, *Pten* might not be epistatic to *Tsc1* in this particular situation, suggesting the diverse relationships between the PI3K/PTEN/AKT and TSC/mTOR pathways.

Although we did observe increased mTOR activity in the later stages (P28) in *Pten* mutants, there was no dramatic cyst formation in adult *Pten* mutants (data not shown). The only abnormality we observed in the kidneys of *Pten* mutants was slightly enlarged kidney size. However, the renal function appeared normal, even when we aged the mice to 1 year of age (data not shown). That *Pten* mutants do not develop PKD could be due to two reasons. First, mTOR activation in *Pten* mutants is less dramatic than in *Tsc1* mutants and occurs in a small percentage of cells, which is true as we demonstrated in this study. Second, there might be a critical timing for the initiation of cyst by mTOR activation. Therefore, although we observed increased mTOR activity at P28, there is sill no dramatic cyst development after a year in *Pten* mutants. Interestingly, this idea is supported by a very recent study in *Pkd1* inducible knockout mice (Piontek et al., 2007). They

observed that inactivation of *Pkd1* in mice before postnatal day 13 resulted in severely polycystic kidney within 3 weeks, whereas inactivation of *Pkd1*after postnatal day 14 resulted in cysts only after 5 month. However, whether this is true in our system needs further evaluation.

References:

(1993). Identification and characterization of the tuberous sclerosis gene on chromosome 16. Cell *75*, 1305-1315.

(1994). The polycystic kidney disease 1 gene encodes a 14 kb transcript and lies within a duplicated region on chromosome 16. The European Polycystic Kidney Disease Consortium. Cell *77*, 881-894.

(1995). Polycystic kidney disease: the complete structure of the PKD1 gene and its protein. The International Polycystic Kidney Disease Consortium. Cell *81*, 289-298.

Alessi, D. R., Andjelkovic, M., Caudwell, B., Cron, P., Morrice, N., Cohen, P., and Hemmings, B. A. (1996). Mechanism of activation of protein kinase B by insulin and IGF-1. Embo J *15*, 6541-6551.

Alessi, D. R., James, S. R., Downes, C. P., Holmes, A. B., Gaffney, P. R., Reese, C. B., and Cohen, P. (1997). Characterization of a 3-phosphoinositide-dependent protein kinase which phosphorylates and activates protein kinase Balpha. Curr Biol *7*, 261-269.

Ali, I. U., Schriml, L. M., and Dean, M. (1999). Mutational spectra of PTEN/MMAC1 gene: a tumor suppressor with lipid phosphatase activity. J Natl Cancer Inst *91*, 1922-1932.

Aman, M. G., and Langworthy, K. S. (2000). Pharmacotherapy for hyperactivity in children with autism and other pervasive developmental disorders. J Autism Dev Disord *30*, 451-459.

Amir, R. E., Van den Veyver, I. B., Wan, M., Tran, C. Q., Francke, U., and Zoghbi, H. Y. (1999). Rett syndrome is caused by mutations in X-linked MECP2, encoding methyl-CpG-binding protein 2. Nat Genet *23*, 185-188.

Baba, M., Furihata, M., Hong, S. B., Tessarollo, L., Haines, D. C., Southon, E., Patel, V., Igarashi, P., Alvord, W. G., Leighty, R., *et al.* (2008). Kidney-targeted Birt-Hogg-Dube gene inactivation in a mouse model: Erk1/2 and Akt-mTOR activation, cell hyperproliferation, and polycystic kidneys. J Natl Cancer Inst *100*, 140-154.

Backman, S. A., Stambolic, V., Suzuki, A., Haight, J., Elia, A., Pretorius, J., Tsao, M. S., Shannon, P., Bolon, B., Ivy, G. O., and Mak, T. W. (2001). Deletion of Pten in mouse brain causes seizures, ataxia and defects in soma size resembling Lhermitte-Duclos disease. Nat Genet *29*, 396-403.

Bagni, C., and Greenough, W. T. (2005). From mRNP trafficking to spine dysmorphogenesis: the roots of fragile X syndrome. Nat Rev Neurosci *6*, 376-387.

Bailey, A., Le Couteur, A., Gottesman, I., Bolton, P., Simonoff, E., Yuzda, E., and Rutter, M. (1995). Autism as a strongly genetic disorder: evidence from a British twin study. Psychol Med *25*, 63-77.

Bellacosa, A., Testa, J. R., Staal, S. P., and Tsichlis, P. N. (1991). A retroviral oncogene, akt, encoding a serine-threonine kinase containing an SH2-like region. Science *254*, 274-277.

Bertrand, J., Mars, A., Boyle, C., Bove, F., Yeargin-Allsopp, M., and Decoufle, P. (2001). Prevalence of autism in a United States population: the Brick Township, New Jersey, investigation. Pediatrics *108*, 1155-1161.

Bolton, P. F., Dennis, N. R., Browne, C. E., Thomas, N. S., Veltman, M. W., Thompson, R. J., and Jacobs, P. (2001). The phenotypic manifestations of interstitial duplications of proximal 15q with special reference to the autistic spectrum disorders. Am J Med Genet *105*, 675-685.

Brook-Carter, P. T., Peral, B., Ward, C. J., Thompson, P., Hughes, J., Maheshwar, M. M., Nellist, M., Gamble, V., Harris, P. C., and Sampson, J. R. (1994). Deletion of the TSC2 and PKD1 genes associated with severe infantile polycystic kidney disease--a contiguous gene syndrome. Nat Genet *8*, 328-332.

Butler, M. G., Dasouki, M. J., Zhou, X. P., Talebizadeh, Z., Brown, M., Takahashi, T. N., Miles, J. H., Wang, C. H., Stratton, R., Pilarski, R., and Eng, C. (2005). Subset of individuals with autism spectrum disorders and extreme macrocephaly associated with germline PTEN tumour suppressor gene mutations. J Med Genet *42*, 318-321.

Cai, S., Everitt, J. I., Kugo, H., Cook, J., Kleymenova, E., and Walker, C. L. (2003). Polycystic kidney disease as a result of loss of the tuberous sclerosis 2 tumor suppressor gene during development. Am J Pathol *162*, 457-468.

Canitano, R. (2007). Epilepsy in autism spectrum disorders. Eur Child Adolesc Psychiatry *16*, 61-66.

Chahrour, M., and Zoghbi, H. Y. (2007). The story of Rett syndrome: from clinic to neurobiology. Neuron *56*, 422-437.

Chemelli, R. M., Willie, J. T., Sinton, C. M., Elmquist, J. K., Scammell, T., Lee, C., Richardson, J. A., Williams, S. C., Xiong, Y., Kisanuki, Y., *et al.* (1999). Narcolepsy in orexin knockout mice: molecular genetics of sleep regulation. Cell *98*, 437-451.

Cook, E. H., Jr., Courchesne, R., Lord, C., Cox, N. J., Yan, S., Lincoln, A., Haas, R., Courchesne, E., and Leventhal, B. L. (1997). Evidence of linkage between the serotonin transporter and autistic disorder. Mol Psychiatry *2*, 247-250.

Courchesne, E., Pierce, K., Schumann, C. M., Redcay, E., Buckwalter, J. A., Kennedy, D. P., and Morgan, J. (2007). Mapping early brain development in autism. Neuron *56*, 399-413.

Danscher, G., Stoltenberg, M., Bruhn, M., Sondergaard, C., and Jensen, D. (2004). Immersion autometallography: histochemical in situ capturing of zinc ions in catalytic zinc-sulfur nanocrystals. J Histochem Cytochem *52*, 1619-1625.

Davidovitch, M., Patterson, B., and Gartside, P. (1996). Head circumference measurements in children with autism. J Child Neurol *11*, 389-393.

Deutsch, C. K., and Joseph, R. M. (2003). Brief report: cognitive correlates of enlarged head circumference in children with autism. J Autism Dev Disord *33*, 209-215.

Fidler, D. J., Bailey, J. N., and Smalley, S. L. (2000). Macrocephaly in autism and other pervasive developmental disorders. Dev Med Child Neurol *42*, 737-740.

Fombonne, E. (2003). Epidemiological surveys of autism and other pervasive developmental disorders: an update. J Autism Dev Disord *33*, 365-382.

Fombonne, E., Roge, B., Claverie, J., Courty, S., and Fremolle, J. (1999). Microcephaly and macrocephaly in autism. J Autism Dev Disord *29*, 113-119.

Fraser, M. M., Zhu, X., Kwon, C. H., Uhlmann, E. J., Gutmann, D. H., and Baker, S. J. (2004). Pten loss causes hypertrophy and increased proliferation of astrocytes in vivo. Cancer Res *64*, 7773-7779.

Garami, A., Zwartkruis, F. J., Nobukuni, T., Joaquin, M., Roccio, M., Stocker, H., Kozma, S. C., Hafen, E., Bos, J. L., and Thomas, G. (2003). Insulin activation of Rheb, a mediator of mTOR/S6K/4E-BP signaling, is inhibited by TSC1 and 2. Mol Cell *11*, 1457-1466.

Goffin, A., Hoefsloot, L. H., Bosgoed, E., Swillen, A., and Fryns, J. P. (2001). PTEN mutation in a family with Cowden syndrome and autism. Am J Med Genet *105*, 521-524.

Groszer, M., Erickson, R., Scripture-Adams, D. D., Lesche, R., Trumpp, A., Zack, J. A., Kornblum, H. I., Liu, X., and Wu, H. (2001). Negative regulation of neural stem/progenitor cell proliferation by the Pten tumor suppressor gene in vivo. Science *294*, 2186-2189.

Hagerman, R. J. (2006). Lessons from fragile X regarding neurobiology, autism, and neurodegeneration. J Dev Behav Pediatr *27*, 63-74.

Hagerman, R. J., Ono, M. Y., and Hagerman, P. J. (2005). Recent advances in fragile X: a model for autism and neurodegeneration. Curr Opin Psychiatry *18*, 490-496.

Harrington, L. S., Findlay, G. M., Gray, A., Tolkacheva, T., Wigfield, S., Rebholz, H., Barnett, J., Leslie, N. R., Cheng, S., Shepherd, P. R., *et al.* (2004). The TSC1-2 tumor suppressor controls insulin-PI3K signaling via regulation of IRS proteins. J Cell Biol *166*, 213-223.

Heitman, J., Movva, N. R., and Hall, M. N. (1991). Targets for cell cycle arrest by the immunosuppressant rapamycin in yeast. Science *253*, 905-909.

Herman, G. E., Butter, E., Enrile, B., Pastore, M., Prior, T. W., and Sommer, A. (2007). Increasing knowledge of PTEN germline mutations: Two additional patients with autism and macrocephaly. Am J Med Genet A *143*, 589-593.

Igarashi, P., and Somlo, S. (2002). Genetics and pathogenesis of polycystic kidney disease. J Am Soc Nephrol *13*, 2384-2398.

Inoki, K., Li, Y., Zhu, T., Wu, J., and Guan, K. L. (2002). TSC2 is phosphorylated and inhibited by Akt and suppresses mTOR signalling. Nat Cell Biol *4*, 648-657.

Jamain, S., Quach, H., Betancur, C., Rastam, M., Colineaux, C., Gillberg, I. C., Soderstrom, H., Giros, B., Leboyer, M., Gillberg, C., and Bourgeron, T. (2003). Mutations of the X-linked genes encoding neuroligins NLGN3 and NLGN4 are associated with autism. Nat Genet *34*, 27-29.

Jaworski, J., Spangler, S., Seeburg, D. P., Hoogenraad, C. C., and Sheng, M. (2005). Control of dendritic arborization by the phosphoinositide-3'-kinase-Akt-mammalian target of rapamycin pathway. J Neurosci *25*, 11300-11312.

Jiang, H., Guo, W., Liang, X., and Rao, Y. (2005). Both the establishment and the maintenance of neuronal polarity require active mechanisms: critical roles of GSK-3beta and its upstream regulators. Cell *120*, 123-135.

Jones, P. F., Jakubowicz, T., Pitossi, F. J., Maurer, F., and Hemmings, B. A. (1991). Molecular cloning and identification of a serine/threonine protein

kinase of the second-messenger subfamily. Proc Natl Acad Sci U S A *88*, 4171-4175.

Jyonouchi, H., Geng, L., Ruby, A., and Zimmerman-Bier, B. (2005). Dysregulated innate immune responses in young children with autism spectrum disorders: their relationship to gastrointestinal symptoms and dietary intervention. Neuropsychobiology *51*, 77-85.

Kim, W. Y., Zhou, F. Q., Zhou, J., Yokota, Y., Wang, Y. M., Yoshimura, T., Kaibuchi, K., Woodgett, J. R., Anton, E. S., and Snider, W. D. (2006). Essential roles for GSK-3s and GSK-3-primed substrates in neurotrophin-induced and hippocampal axon growth. Neuron *52*, 981-996.

Klauck, S. M. (2006). Genetics of autism spectrum disorder. Eur J Hum Genet *14*, 714-720.

Kleymenova, E., Ibraghimov-Beskrovnaya, O., Kugoh, H., Everitt, J., Xu, H., Kiguchi, K., Landes, G., Harris, P., and Walker, C. (2001). Tuberin-dependent membrane localization of polycystin-1: a functional link between polycystic kidney disease and the TSC2 tumor suppressor gene. Mol Cell *7*, 823-832.

Kobayashi, T., Hirayama, Y., Kobayashi, E., Kubo, Y., and Hino, O. (1995). A germline insertion in the tuberous sclerosis (Tsc2) gene gives rise to the Eker rat model of dominantly inherited cancer. Nat Genet *9*, 70-74.

Kuemerle, B., Gulden, F., Cherosky, N., Williams, E., and Herrup, K. (2007). The mouse Engrailed genes: a window into autism. Behav Brain Res *176*, 121-132.

Kumar, V., Zhang, M. X., Swank, M. W., Kunz, J., and Wu, G. Y. (2005). Regulation of dendritic morphogenesis by Ras-PI3K-Akt-mTOR and Ras-MAPK signaling pathways. J Neurosci *25*, 11288-11299.

Kwon, C. H., Luikart, B. W., Powell, C. M., Zhou, J., Matheny, S. A., Zhang, W., Li, Y., Baker, S. J., and Parada, L. F. (2006a). Pten regulates neuronal arborization and social interaction in mice. Neuron *50*, 377-388.

Kwon, C. H., Zhou, J., Li, Y., Kim, K. W., Hensley, L. L., Baker, S. J., and Parada, L. F. (2006b). Neuron-specific enolase-cre mouse line with cre activity in specific neuronal populations. Genesis *44*, 130-135.

Kwon, C. H., Zhu, X., Zhang, J., and Baker, S. J. (2003). mTor is required for hypertrophy of Pten-deficient neuronal soma in vivo. Proc Natl Acad Sci U S A *100*, 12923-12928.

Kwon, C. H., Zhu, X., Zhang, J., Knoop, L. L., Tharp, R., Smeyne, R. J., Eberhart, C. G., Burger, P. C., and Baker, S. J. (2001). Pten regulates neuronal soma size: a mouse model of Lhermitte-Duclos disease. Nat Genet *29*, 404-411.

Lainhart, J. E. (2003). Increased rate of head growth during infancy in autism. Jama *290*, 393-394.

Lainhart, J. E., Piven, J., Wzorek, M., Landa, R., Santangelo, S. L., Coon, H., and Folstein, S. E. (1997). Macrocephaly in children and adults with autism. J Am Acad Child Adolesc Psychiatry *36*, 282-290.

Li, J., Yen, C., Liaw, D., Podsypanina, K., Bose, S., Wang, S. I., Puc, J., Miliaresis, C., Rodgers, L., McCombie, R., *et al.* (1997). PTEN, a putative

protein tyrosine phosphatase gene mutated in human brain, breast, and prostate cancer. Science *275*, 1943-1947.

Long, X., Lin, Y., Ortiz-Vega, S., Yonezawa, K., and Avruch, J. (2005). Rheb binds and regulates the mTOR kinase. Curr Biol *15*, 702-713.

Luikart, B. W., Nef, S., Virmani, T., Lush, M. E., Liu, Y., Kavalali, E. T., and Parada, L. F. (2005). TrkB has a cell-autonomous role in the establishment of hippocampal Schaffer collateral synapses. J Neurosci *25*, 3774-3786.

Maehama, T., and Dixon, J. E. (1998). The tumor suppressor, PTEN/MMAC1, dephosphorylates the lipid second messenger, phosphatidylinositol 3,4,5-trisphosphate. J Biol Chem *273*, 13375-13378.

Malow, B. A. (2004). Sleep disorders, epilepsy, and autism. Ment Retard Dev Disabil Res Rev *10*, 122-125.

Manning, B. D., and Cantley, L. C. (2007). AKT/PKB signaling: navigating downstream. Cell *129*, 1261-1274.

Manning, B. D., Tee, A. R., Logsdon, M. N., Blenis, J., and Cantley, L. C. (2002). Identification of the tuberous sclerosis complex-2 tumor suppressor gene product tuberin as a target of the phosphoinositide 3-kinase/akt pathway. Mol Cell *10*, 151-162.

Marsh, D. J., Kum, J. B., Lunetta, K. L., Bennett, M. J., Gorlin, R. J., Ahmed, S. F., Bodurtha, J., Crowe, C., Curtis, M. A., Dasouki, M., *et al.* (1999). PTEN mutation spectrum and genotype-phenotype correlations in Bannayan-Riley-Ruvalcaba syndrome suggest a single entity with Cowden syndrome. Hum Mol Genet *8*, 1461-1472.

Meikle, L., Pollizzi, K., Egnor, A., Kramvis, I., Lane, H., Sahin, M., and Kwiatkowski, D. J. (2008). Response of a neuronal model of tuberous sclerosis to mammalian target of rapamycin (mTOR) inhibitors: effects on mTORC1 and Akt signaling lead to improved survival and function. J Neurosci *28*, 5422-5432.

Meikle, L., Talos, D. M., Onda, H., Pollizzi, K., Rotenberg, A., Sahin, M., Jensen, F. E., and Kwiatkowski, D. J. (2007). A mouse model of tuberous sclerosis: neuronal loss of Tsc1 causes dysplastic and ectopic neurons, reduced myelination, seizure activity, and limited survival. J Neurosci *27*, 5546-5558.

Mochizuki, T., Wu, G., Hayashi, T., Xenophontos, S. L., Veldhuisen, B., Saris, J. J., Reynolds, D. M., Cai, Y., Gabow, P. A., Pierides, A., *et al.* (1996). PKD2, a gene for polycystic kidney disease that encodes an integral membrane protein. Science *272*, 1339-1342.

Muhle, R., Trentacoste, S. V., and Rapin, I. (2004). The genetics of autism. Pediatrics *113*, e472-486.

Nauli, S. M., Alenghat, F. J., Luo, Y., Williams, E., Vassilev, P., Li, X., Elia, A. E., Lu, W., Brown, E. M., Quinn, S. J., *et al.* (2003). Polycystins 1 and 2 mediate mechanosensation in the primary cilium of kidney cells. Nat Genet *33*, 129-137.

Ogawa, S., Kwon, C. H., Zhou, J., Koovakkattu, D., Parada, L. F., and Sinton, C. M. (2007). A seizure-prone phenotype is associated with altered free-running rhythm in Pten mutant mice. Brain Res *1168*, 112-123.

Osborne, J. P., Fryer, A., and Webb, D. (1991). Epidemiology of tuberous sclerosis. Ann N Y Acad Sci *615*, 125-127.

Pende, M., Um, S. H., Mieulet, V., Sticker, M., Goss, V. L., Mestan, J., Mueller, M., Fumagalli, S., Kozma, S. C., and Thomas, G. (2004). S6K1(-/-)/S6K2(-/-) mice exhibit perinatal lethality and rapamycin-sensitive 5'-terminal oligopyrimidine mRNA translation and reveal a mitogen-activated protein kinase-dependent S6 kinase pathway. Mol Cell Biol *24*, 3112-3124.

Percy, A. K. (2002). Rett syndrome. Current status and new vistas. Neurol Clin *20*, 1125-1141.

Piontek, K., Menezes, L. F., Garcia-Gonzalez, M. A., Huso, D. L., and Germino, G. G. (2007). A critical developmental switch defines the kinetics of kidney cyst formation after loss of Pkd1. Nat Med *13*, 1490-1495.

Piven, J., Arndt, S., Bailey, J., Havercamp, S., Andreasen, N. C., and Palmer, P. (1995). An MRI study of brain size in autism. Am J Psychiatry *152*, 1145-1149.

Potter, C. J., Pedraza, L. G., and Xu, T. (2002). Akt regulates growth by directly phosphorylating Tsc2. Nat Cell Biol *4*, 658-665.

Richter, J. D., and Sonenberg, N. (2005). Regulation of cap-dependent translation by eIF4E inhibitory proteins. Nature *433*, 477-480.

Sabatini, D. M., Erdjument-Bromage, H., Lui, M., Tempst, P., and Snyder, S. H. (1994). RAFT1: a mammalian protein that binds to FKBP12 in a rapamycin-dependent fashion and is homologous to yeast TORs. Cell *78*, 35-43.

Sampson, J. R., Maheshwar, M. M., Aspinwall, R., Thompson, P., Cheadle, J. P., Ravine, D., Roy, S., Haan, E., Bernstein, J., and Harris, P. C. (1997). Renal

cystic disease in tuberous sclerosis: role of the polycystic kidney disease 1 gene. Am J Hum Genet *61*, 843-851.

Sansal, I., and Sellers, W. R. (2004). The biology and clinical relevance of the PTEN tumor suppressor pathway. J Clin Oncol *22*, 2954-2963.

Sarbassov, D. D., Ali, S. M., Sengupta, S., Sheen, J. H., Hsu, P. P., Bagley, A. F., Markhard, A. L., and Sabatini, D. M. (2006). Prolonged rapamycin treatment inhibits mTORC2 assembly and Akt/PKB. Mol Cell *22*, 159-168.

Sarbassov, D. D., Guertin, D. A., Ali, S. M., and Sabatini, D. M. (2005). Phosphorylation and regulation of Akt/PKB by the rictor-mTOR complex. Science *307*, 1098-1101.

Saucedo, L. J., Gao, X., Chiarelli, D. A., Li, L., Pan, D., and Edgar, B. A. (2003). Rheb promotes cell growth as a component of the insulin/TOR signalling network. Nat Cell Biol *5*, 566-571.

Serajee, F. J., Zhong, H., and Mahbubul Huq, A. H. (2006). Association of Reelin gene polymorphisms with autism. Genomics *87*, 75-83.

Shah, O. J., Wang, Z., and Hunter, T. (2004). Inappropriate activation of the TSC/Rheb/mTOR/S6K cassette induces IRS1/2 depletion, insulin resistance, and cell survival deficiencies. Curr Biol *14*, 1650-1656.

Shillingford, J. M., Murcia, N. S., Larson, C. H., Low, S. H., Hedgepeth, R., Brown, N., Flask, C. A., Novick, A. C., Goldfarb, D. A., Kramer-Zucker, A., *et al.* (2006). The mTOR pathway is regulated by polycystin-1, and its inhibition reverses renal cystogenesis in polycystic kidney disease. Proc Natl Acad Sci U S A *103*, 5466-5471.

Smalley, S. L. (1998). Autism and tuberous sclerosis. J Autism Dev Disord *28*, 407-414.

Smalley, S. L., Tanguay, P. E., Smith, M., and Gutierrez, G. (1992). Autism and tuberous sclerosis. J Autism Dev Disord *22*, 339-355.

Soriano, P. (1999). Generalized lacZ expression with the ROSA26 Cre reporter strain. Nat Genet *21*, 70-71.

Srinivas, S., Watanabe, T., Lin, C. S., William, C. M., Tanabe, Y., Jessell, T. M., and Costantini, F. (2001). Cre reporter strains produced by targeted insertion of EYFP and ECFP into the ROSA26 locus. BMC Dev Biol *1*, 4.

Staal, S. P. (1987). Molecular cloning of the akt oncogene and its human homologues AKT1 and AKT2: amplification of AKT1 in a primary human gastric adenocarcinoma. Proc Natl Acad Sci U S A *84*, 5034-5037.

Steck, P. A., Pershouse, M. A., Jasser, S. A., Yung, W. K., Lin, H., Ligon, A. H., Langford, L. A., Baumgard, M. L., Hattier, T., Davis, T., *et al.* (1997). Identification of a candidate tumour suppressor gene, MMAC1, at chromosome 10q23.3 that is mutated in multiple advanced cancers. Nat Genet *15*, 356-362.

Stevenson, R. E., Schroer, R. J., Skinner, C., Fender, D., and Simensen, R. J. (1997). Autism and macrocephaly. Lancet *349*, 1744-1745.

Stocker, H., Radimerski, T., Schindelholz, B., Wittwer, F., Belawat, P., Daram, P., Breuer, S., Thomas, G., and Hafen, E. (2003). Rheb is an essential regulator of S6K in controlling cell growth in Drosophila. Nat Cell Biol *5*, 559-565.

Stokoe, D., Stephens, L. R., Copeland, T., Gaffney, P. R., Reese, C. B., Painter, G. F., Holmes, A. B., McCormick, F., and Hawkins, P. T. (1997). Dual role of phosphatidylinositol-3,4,5-trisphosphate in the activation of protein kinase B. Science *277*, 567-570.

Stolovich, M., Tang, H., Hornstein, E., Levy, G., Cohen, R., Bae, S. S., Birnbaum, M. J., and Meyuhas, O. (2002). Transduction of growth or mitogenic signals into translational activation of TOP mRNAs is fully reliant on the phosphatidylinositol 3-kinase-mediated pathway but requires neither S6K1 nor rpS6 phosphorylation. Mol Cell Biol *22*, 8101-8113.

Tabuchi, K., Blundell, J., Etherton, M. R., Hammer, R. E., Liu, X., Powell, C. M., and Sudhof, T. C. (2007). A neuroligin-3 mutation implicated in autism increases inhibitory synaptic transmission in mice. Science *318*, 71-76.

Tavazoie, S. F., Alvarez, V. A., Ridenour, D. A., Kwiatkowski, D. J., and Sabatini, B. L. (2005). Regulation of neuronal morphology and function by the tumor suppressors Tsc1 and Tsc2. Nat Neurosci *8*, 1727-1734.

Tee, A. R., and Blenis, J. (2005). mTOR, translational control and human disease. Semin Cell Dev Biol *16*, 29-37.

Tee, A. R., Manning, B. D., Roux, P. P., Cantley, L. C., and Blenis, J. (2003). Tuberous sclerosis complex gene products, Tuberin and Hamartin, control mTOR signaling by acting as a GTPase-activating protein complex toward Rheb. Curr Biol *13*, 1259-1268.

Torres, V. E., and Harris, P. C. (2006). Mechanisms of Disease: autosomal dominant and recessive polycystic kidney diseases. Nat Clin Pract Nephrol *2*, 40-55; quiz 55.

Tuchman, R., and Rapin, I. (2002). Epilepsy in autism. Lancet Neurol *1*, 352-358.

Ulfig, N., Nickel, J., and Bohl, J. (1998). Monoclonal antibodies SMI 311 and SMI 312 as tools to investigate the maturation of nerve cells and axonal patterns in human fetal brain. Cell Tissue Res *291*, 433-443.

Um, S. H., Frigerio, F., Watanabe, M., Picard, F., Joaquin, M., Sticker, M., Fumagalli, S., Allegrini, P. R., Kozma, S. C., Auwerx, J., and Thomas, G. (2004). Absence of S6K1 protects against age- and diet-induced obesity while enhancing insulin sensitivity. Nature *431*, 200-205.

Valicenti-McDermott, M., McVicar, K., Rapin, I., Wershil, B. K., Cohen, H., and Shinnar, S. (2006). Frequency of gastrointestinal symptoms in children with autistic spectrum disorders and association with family history of autoimmune disease. J Dev Behav Pediatr *27*, S128-136.

van Slegtenhorst, M., de Hoogt, R., Hermans, C., Nellist, M., Janssen, B., Verhoef, S., Lindhout, D., van den Ouweland, A., Halley, D., Young, J., *et al.* (1997). Identification of the tuberous sclerosis gene TSC1 on chromosome 9q34. Science *277*, 805-808.

Vezina, C., Kudelski, A., and Sehgal, S. N. (1975). Rapamycin (AY-22,989), a new antifungal antibiotic. I. Taxonomy of the producing streptomycete and isolation of the active principle. J Antibiot (Tokyo) *28*, 721-726.

Vivanco, I., and Sawyers, C. L. (2002). The phosphatidylinositol 3-Kinase AKT pathway in human cancer. Nat Rev Cancer *2*, 489-501.

Wassink, T. H., Brzustowicz, L. M., Bartlett, C. W., and Szatmari, P. (2004). The search for autism disease genes. Ment Retard Dev Disabil Res Rev *10*, 272-283.

Wilson, P. D. (2004). Polycystic kidney disease. N Engl J Med *350*, 151-164.

Wiznitzer, M. (2004). Autism and tuberous sclerosis. J Child Neurol *19*, 675-679.

Wullschleger, S., Loewith, R., and Hall, M. N. (2006). TOR signaling in growth and metabolism. Cell *124*, 471-484.

Yeargin-Allsopp, M., Rice, C., Karapurkar, T., Doernberg, N., Boyle, C., and Murphy, C. (2003). Prevalence of autism in a US metropolitan area. Jama *289*, 49-55.

Yirmiya, N., Pilowsky, T., Nemanov, L., Arbelle, S., Feinsilver, T., Fried, I., and Ebstein, R. P. (2001). Evidence for an association with the serotonin transporter promoter region polymorphism and autism. Am J Med Genet *105*, 381-386.

Zhang, Y., Gao, X., Saucedo, L. J., Ru, B., Edgar, B. A., and Pan, D. (2003). Rheb is a direct target of the tuberous sclerosis tumour suppressor proteins. Nat Cell Biol *5*, 578-581.